Genomic meta-analysis of the interplay between 3D chromatin organization and gene expression programs under basal and stress conditions

Idan Nurick[1,2], Ron Shamir[1*] and Ran Elkon[2*]

[1]The Blavatnik School of Computer Science, Tel Aviv University, Tel Aviv, Israel.

[2] Department of Human Molecular Genetics and Biochemistry, Sackler School of Medicine, Tel Aviv University, Tel Aviv, Israel.

* equal contribution.

Emails

Idan Nurick idan.nurick@gmail.com
Ron Shamir rshamir@tau.ac.il
Ran Elkon ranel@tauex.tau.ac.il

Corresponding authors

Ron Shamir
rshamir@tau.ac.il
Blavatnik School of Computer Science
Tel Aviv University,
Tel Aviv, 69978, Israel

Ran Elkon
ranel@tauex.tau.ac.il
Department of Human Molecular Genetics & Biochemistry
Sackler School of Medicine
Tel Aviv University
Tel Aviv 69978, Israel

Abstract (350 words)

Background. Our appreciation of the critical role of the 3D organization of the genome in gene regulation is steadily increasing. Recent 3C-based deep sequencing techniques elucidated a hierarchy of structures that underlie the spatial organization of the genome in the nucleus. At the top of this hierarchical organization are chromosomal territories and the megabase-scale A/B compartments that correlate with transcriptional activity within cells. Below them are the relatively cell-type invariant topologically associated domains (TADs), characterized by high frequency of physical contacts between loci within the same TAD and are assumed to function as regulatory units. Within TADs, chromatin loops bring enhancers and target promoters to close spatial proximity. Yet, we still have only rudimentary understanding how differences in chromatin organization between different cell types affect cell-type specific gene expression programs that are executed under basal and challenged conditions.

Results. Here, we carried out a large-scale meta-analysis that integrated Hi-C data from thirteen different cell lines and dozens of ChIP-seq and RNA-seq datasets measured on these cells, either under basal conditions or after treatment. Pairwise comparisons between cell lines demonstrated the strong association between modulation of A/B compartmentalization, differential gene expression and transcription factor (TF) binding events. Furthermore, integrating the analysis of transcriptomes of different cell lines in response to various challenges, we show that 3D organization of cells under basal conditions constrains not only gene expression programs and TF binding profiles that are active under the basal condition but also those induced in response to treatment.

Conclusions. Our results further elucidate the role of dynamic genome organization in regulation of differential gene expression between different cell types, and indicate the impact of intra-TAD enhancer-promoter interactions that are established under basal conditions on both the basal and treatment-induced gene expression programs.

Keywords: 3D genome organization; gene regulation; meta-analysis; A/B compartments; Enhancer-promoter interactions

Background

3C-based methods measure the frequency of physical interactions between any pair of genomic loci as a proxy for their spatial proximity. These novel technologies are shedding light on the principles of 3D organization of the genome in the nucleus and its relation to gene regulation [1-3]. A four-layer hierarchy of structures is emerging from these studies [4, 5]. At the top of this hierarchy are the chromosomes which are generally organized in a way that gene-dense chromosomes tend to be at the nuclear interior whereas the more gene-poor chromosomes are found near the nuclear periphery [6]. In the next layer are megabase-scale genomic compartments that are either euchromatic, gene-rich, and transcriptionally active (called A compartments) or heterochromatic, gene-poor, and transcriptionally silent (called B compartments) [5, 7]. Spatially, the open (A-type) compartments cluster together in the nuclear interior, whereas the closed (B-type) compartments tend to cluster near the nuclear periphery [4]. These chromosomal compartments contain ~100kb-1Mb scale subunits called topologically associating domains (TADs). These are characterized by high frequency of interactions between loci located in the same domain, and much lower interaction rate between loci located in adjacent TADs [8, 9]. Unlike the A/B compartments, which associate to gene expression and therefore markedly vary between different cell types, TADs are largely invariant across different cell types and physiological conditions [7, 10]. At the bottom of the hierarchy are ~10Kb-1Mb chromatin-looping interactions, bringing enhancers (E) and promoters (P) that are located at high distance along the linear DNA sequence to close spatial proximity. Such E-P loops, a portion of which is cell type specific, mostly occur within TADs and unfrequently cross over TAD boundaries [4, 10]. The 3D organization of the genome has a pronounced cell-to-cell stochastic variability, and the snapshots obtained by 3C-based analyses are typically the result of averaging over a large ensemble of cells.

Our understanding of the roles that the 3D organization of the genome plays in gene regulation has markedly increased in recent years. It emerges that TADs serve as fundamental structural and regulatory building blocks of chromosomes that constrain and largely exclude physical interactions between genes and regulatory elements located in different TADs, while providing sufficiently dynamic local environment that is required for the establishment of intra-TAD E-P links [4, 8]. In line with the view of TADs as

structural regulatory units, examination of the dynamic changes in genome 3D organization during differentiation of stem cells into six different linages showed that the regions that changed their A/B compartment mostly corresponded to a single or a series of adjacent TADs [11]. In addition, no significant changes in TAD boundaries were detected in a breast cancer cell-line upon treatment with hormone, suggesting that TADs are also invariant under transient cell challenges [12]. Furthermore, this study found a statistically significant, though limited, number of TADs that behaved as discrete regulatory units where the majority of the genes inside them were either coordinately induced or repressed.

Intra-TAD E-P links are required for the implementation of transcriptional programs that establish and maintain cell identity and responses to environmental cues. How these regulatory interactions are modulated in response to transient perturbation is still not well understood. While some studies have shown that gene induction is accompanied by alterations of chromatin interactions and internal restructuring of TADs [12-14], unexpectedly, it was recently observed that the majority of TNF-α responsive enhancers were already in contact with their target promoters before treatment [15]. Given that the transcriptional responses to various stresses show high level of cell-type specificity, these results suggest that intra-TAD interactions that are already in place in each cell type under basal conditions affect the spectrum of genes that are induced upon triggers in each cell type.

Here, we carried out a large-scale meta-analysis, integrating Hi-C data from 13 different cell lines and dozens of ChIP-seq and RNA-seq datasets recorded in the same cellular systems at basal conditions and in response to various treatments, to further elucidate the intricate interplay between the hierarchical 3D organization of the genome and gene regulation.

Results

Differences in gene expression between cell lines correlate with A/B compartmentalization

We first defined the higher order organization of the genome into A/B compartments for 13 human cell lines for which Hi-C data are available (**Supplementary Table 1**). We normalized each Hi-C matrix and performed principal component analysis (PCA) for each intra-chromosomal matrix separately (Methods). By definition, the A compartment is gene rich and is broadly associated with active transcription and epigenomic marks of open chromatin, while the B compartment is gene poor and associates with low transcriptional activity and condensed chromatin. Thus, for each chromosome separately, we used gene density to determine if positive or negative values of the PC that represents the A/B compartmentalization corresponds to A compartment. (Centromeric regions were not included in the A/B partitions since no chromatin interactions are identified by Hi-C in these regions.) **Table 1** summarizes the total genomic size and number of genes assigned to the A and B compartments in each cell line. As an example, **Fig. 1A** shows the partition into A/B compartments we obtained for chromosome 1 in the 13 cell lines. On average, 25% of the genome showed assignment to different compartment in pairwise comparisons between cell lines.

As a first examination, per cell line, we confirmed that genes assigned to the A compartment are significantly more highly expressed than genes assigned to the B compartment (**Fig. 1B**). Next, we tested for association between differences in A/B compartmentalization and gene expression across different cell lines. Specifically, for each pair of cell lines, we examined whether genes located in A compartment in one cell line and in B compartment in the other show higher expression in the former. Thus, for each pair of cell lines, we divided the genes into four sets – A in both cell lines (AA), B in both cell lines (BB), A in cell line 1 and B in cell line 2 (AB) and B in cell line 1 and A in cell line 2 (BA). We calculated gene-expression ratios between cell line 1 and 2 and compared the distribution of these ratios between the four gene sets. This analysis confirmed that genes in the AB set are significantly more highly expressed in cell line 1, while genes in the BA set show significantly higher expression in cell line 2 (**Fig. 1C; Fig. S1**).

Epigenetic differences between cell lines correlate with differences in A/B compartmentalization

As the A compartment is associated with open state of the chromatin we next systematically examined the association between A/B compartmentalization and TF binding. We analyzed 122 TF ChIP-seq datasets recorded by ENCODE for cell lines with Hi-C data (**Supplementary Table 2**). First, we measured TF binding site (TFBS) enrichment for the A compartment, for each cell line separately, by defining the *A-B density factor, D* ($D > 1$ implies that binding sites are enriched for the A compartment and $D < 1$ implies that binding sites are enriched for B compartment; Methods). As expected, the chromatin-binding profile of all TFs in all examined cell lines showed a remarkable enrichment for the A compartment (**Fig. S2**; see **Supplementary Table 3** for one detailed example: CTCF).

Next, we examined if A-B transitions between cell-lines are reflected by TF binding profiles. For each pair of cell lines, numbered 1 and 2, we segmented the genome into four regions according to A/B assignment in the two cell lines as described above. For a given TF, we divided the TF binding sites into three groups: sites common to cell line 1 and 2, sites detected only in cell line 1 and sites detected only in cell line 2. We then tested for a relationship between these two divisions. Specifically, we defined the *A-B occupancy enrichment ratio R* (see Methods) to test whether cell-type specific TFBSs occur more often in regions assigned as A compartment in the cell line where the binding occurs and as B in the other cell line than the opposite regions (that is, regions assigned as B-type in the cell line where the binding occurs and as A in the other one). **Table 2A** shows, as an example, the results obtained for CTCF binding sites in the comparison between the HMEC and HUVEC cell lines. As expected, we observed that CTCF BSs specific to HMEC (HUVEC) showed significant preference to AB (BA) genomic regions over BA (AB) regions. As CTCF ChIP-seq data were available for six cell lines with Hi-C data, we could systematically carry out this comparison for this factor. In all pairwise tests, we observed a highly significant preference of CTCF cell-type specific binding to cell-type specific A over B regions (**Fig. 2A**). Yet, a large portion of cell-type specific TFBSs were located in genomic regions that are assigned to A compartment in both cell lines (AA regions) (**Table**

2A), indicating that other factors in addition to A/B compartmentalization determine the TF-chromatin interaction profile in each cell type.

To study the relation between cell-type specific binding sites and compartments across many TFs, we focused on GM12878 and K562, which have ChIP-seq data for 49 common TFs. Strong cell-type specific TFBS-compartment relationship was observed for the vast majority of TFs (**Fig. 2B**). We obtained a significant relationship for 44 out of 49 TFs (FDR < 0.05). (Three out of the five TFs with non-significant p-value have very small group sizes and thus their tests lack statistical power.) The strongest effect was observed for EP300, a transcriptional activator that marks active enhancers.

Next, we carried out similar tests for selected epigenetic marks. H3K9ac, which marks transcriptionally active regions, showed the same correlation between cell-type specific signal and compartmentalization (**Table 2B; Supplementary Table 4A**). Notably, the opposite trend was observed for H3K27me3, which is an epigenetic mark of transcriptionally silenced regions. Namely, in pairwise comparisons between cell lines, regions that showed H3K27me3 signal in only cell line 1 were preferentially associated with BA regions (that is, regions assigned to B compartment in cell line1 and A – in cell line 2) over AB regions (**Table 2C; Supplementary Table 4B**).

Association between extent of promoter interactions and basal gene expression

The A compartment is generally characterized by high transcriptional activity. Yet, genes within this compartment show considerable expression variability and many of them are not expressed at any detectable level. Our next analysis thus focused on genes within the A compartment, and examined the relationship between the extent of chromatin interactions at promoter regions and gene expression level. In this analysis, we used promoter-enhancer interactions inferred from Hi-C data by the PSYCHIC tool [16]. We expected that, per cell type, promoters of highly expressed genes would show stronger engagement in chromatin interactions than promoters of lowly expressed genes. Indeed, in all five cell lines that we tested, we found a significant positive association between the number of interactions in which a promoter is involved and the gene's expression level (**Fig. 3A-B; Fig. S3A-B**). We next applied a similar test, but this time using experimental

promoter interactions derived from ENCODE's ChIA-PET data for RNA polymerase II in three cell lines (K562, GM12878 and MCF7). Here too, for all three cell lines examined, we a found a highly significant positive association between extent of promoter interactions and gene expression level (**Fig. 3C-D**; **Fig. S3C-D**).

The above analysis was done on each cell line separately. We next examined correlation between dynamic promoter interactions and gene expression across cell lines. Specifically, we tested if changes in a gene's expression over different cell lines are associated with differences in the number of interactions involving the gene's promoter in these cell lines. This analysis too was confined to genes located within the A compartment in both cell lines ("AA" genes). For each pair of cell lines, we divided the genes into four groups, based on RNA Pol-II ChIA-PET data: no promoter interactions in both cells ("00" group); promoter interactions detected only in cell line 1 ("10" genes); only in cell line 2 ("01" genes) and in both ("11" genes). Notably, differential gene expression between pairs of cell lines was strongly associated with differential engagement of promoters in chromatin interactions (**Fig. 4A-B** for MCF7 vs. K562). Similar results were obtained for the other pairs that we examined (data not shown). These results indicate that dynamic, intra TAD chromatin interactions involving gene promoters within the A compartment modulate cell-type specific gene expression.

Association between basal chromatin organization and treatment-induced TF binding profiles

Many transcriptomic studies demonstrated that a large portion of the transcriptional response to various challenges is cell-type specific [17-19]. Surprisingly, recent epigenomic and transcriptomic analysis of the response to TNFα observed that enhancers activated by this trigger were already in contact with their target promoters before treatment [15]. Therefore, we next sought to examine the role of basal chromatin interactions, which are in place in cells before any challenge is applied, in shaping cell-type responses induced by treatment. To allow us to draw general conclusions, we analyzed a variety of cell lines and multiple treatments covering diverse biological processes. We first analyzed 110 publicly available ChIP-seq datasets, recorded in cells for which we analyzed Hi-C data,

that profiled TF binding and epigenetic marks before and after the application of various treatments. Overall, we analyzed 21 TFs in seven cell lines in response to 22 treatments. Per experiment, we analyzed TFBSs detected under basal and stress conditions and identified the set of TFBSs that were induced in response to treatment. We then divided these induced TFBSs into A/B compartments. For the vast majority of experiments (>90%), we observed a highly significant preference of the induced sites to the A compartment, indicating that the preexisting A/B compartmentalization within a cell line constrains TF-chromatin interactions that are induced in response to stress **(Fig. 5A** and **Supplementary Table** 5).

Next, to examine the relationship between cell-type specific chromatin organization and response to treatment more directly, we sought ChIP-seq datasets that profiled the same TF in response to the same treatment in different cell lines (for which we also analyzed Hi-C data). Several experiments that examined responses to TNFα and estradiol met this requirement. For each pair of cell lines treated by the same agent and profiled for the same TF, we again divided the induced TFBSs into three groups: binding sites induced upon treatment only in cell line 1, binding sites induced only in cell line 2 and binding sites induced in both. Induced TFBSs in each group were then divided into four categories – AA, AB, BA and BB as defined above. In all comparisons, TFBSs induced only in cell line 1 showed significant preference for AB regions over the BA ones, and vice versa for TFBSs induced only in cell line 2 (**Table 3**; **Supplementary Table 6**). This result further demonstrates the impact of cell-specific basal genome organization on the landscape of TF-chromatin interactions that are induced upon challenge. Note that despite the significant association between cell-type specific TF binding induction and chromatin organization, most of the cell-type specific induced TFBSs were located in AA regions (**Table 3**; **Supplementary Table 6**), indicating that factors other than A/B compartmentalization play more dominant role in determining cell-type specific TF binding profiles.

Association between basal chromatin organization and transcriptional response to treatment

The above analyses examined the association between basal chromatin 3D organization and treatment-induced TF-chromatin interactions. Next, we examined the

association between basal chromatin 3D organization and gene induction in response to treatment. For this goal, we analyzed 36 gene expression datasets that recorded transcriptome profiles in response to various challenges (in cell lines for which we have analyzed Hi-C data). For each cell line and treatment, we tested if the set of genes that were induced upon treatment was over-represented in the A compartment. Indeed, in most conditions, we observed a significant preference of the induced genes to the A compartment (**Fig. 5B** and **Supplementary Table 7**). This suggests that the preference of induced TFBSs to the pre-challenge A compartment leads to an induced transcriptional response that show similar preference. The statistical significance obtained by the analysis of the induced genes was usually lower than that obtained by the induced TFBSs since the numbers of responsive genes were substantially lower than the numbers of induced TFBSs. Nevertheless, 28 out of 34 experiments had a significant p-value (FDR < 0.05) and 32 out of 34 experiments had enrichment factor larger than 1.0 ($p < 3.5 * 10^{-8}$; binomial test).

In a previous section, we described an association between the extent of promoter interactions and basal gene expression level (**Fig. 3**). Here, we examined if promoters of genes, within compartment A, that were induced in response to challenges also show higher involvement in chromatin interactions that already exist in the cells under basal condition. Analyzing numerous RNA-seq datasets, we systematically observed that promoters of induced genes were engaged, already in basal conditions, in a markedly higher number of chromatin interactions compared to promoters of non-induced genes that are located in the A compartment and have comparable basal expression levels. We estimated the significance of this higher degree of chromatin interaction by using a permutation test with 10,000 iterations, in each iteration selecting a random set of genes (from A compartment) of the same size as the induced genes set. Expression level was controlled for by dividing the A-compartment genes into 10 bins, according to their basal expression level, and generating random gene sets having the same distribution as the test set of the induced gene. In all experiments except one (with very low number of included genes and thus limited statistical power), we obtained significant p-values ($p<0.05$) (**Fig. 6**; **Supplementary Table 8**).

Last, we examined if cell-type specific gene induction in response to treatment correlates with pre-existing chromatin compartmentalization. We focused on response to

TNFα as we gathered RNA-seq datasets that profiled responses to this trigger in five different cell lines for which we determined AB compartmentalization based on Hi-C data (HMEC, IMR90, GM12878, MCF7 and HUVEC). We followed the same analysis that we applied above to TFBSs that were induced in a cell-type specific manner (Table 3), and applied it to the set of TNFα-induced genes. For 8 out of 10 pairwise comparisons we found a strong association: genes induced specifically in cell line 1 were significantly enriched for AB over BA regions (and vice versa for genes specifically induced in cell line 2) (**Table 4; Supplementary Table 9**). Notably, in this analysis too, the majority of cell-type specific responsive genes were located in AA regions, again indicating that other factors play critical roles in determining the specific spectrum of genes that respond to a challenge in each cell type.

Discussion

To further explore links between the 3D organization of the genome and gene regulation, we have analyzed together Hi-C data from 13 different human cell lines and numerous ChIP-seq and RNA-seq experiments that were recorded in the same cell lines under basal conditions and in response to various treatments. We first confirmed the strong relationship between the partition of the genome into the A/B compartments and transcriptional activity. In all cell lines, expression level of genes located within the A compartment was significantly higher than expression level of genes located in B (**Fig. 1B**), and differential expression between cell lines correlated with differences in AB compartmentalization (**Fig. 1C**). Similarly, in analysis of 122 TF ChIP-seq datasets, the binding profile of the vast majority of TFs showed a significant preference for the A compartment (**Fig. S2**), and cell-type specific TF binding events correlated with cell-type specific A compartments (**Fig. 2**). As expected, the H3K27me3 epigenetic modification that marks transcriptionally silenced regions showed the opposite preference and was highly enriched in the B compartment (**Table 2C**). These results demonstrate the effect of higher order chromosomal organization on TF-chromatin interaction profiles. Yet, in comparisons of TF binding profiles between different cell lines, the majority of cell-type specific TFBSs were located in genomic regions that are assigned to A compartment in both cell lines (AA regions) (**Table 2**). This observation indicates that other factors play

stronger roles than A/B compartmentalization in shaping the landscape of TF-chromatin interactions in each cell type. Master TFs that establish and maintain cell identify are likely a major factor. These regulators exhibit highly cell-type specific expression pattern and were shown to have great impact on the selection of TF binding sites in different cell types [20, 21].

Using E-P links derived from Hi-C and ChIA-PET data, we found a strong correlation between gene expression levels and the extent to which promoters are engaged in chromatin interactions (**Fig. 3**). Moreover, we showed that differential expression between cell types is associated with dynamic change in involvement of promoters in such interactions (**Fig. 4**), which are most likely mediated by cell type specific TFs. A recent study showed that during cell reprogramming, the expression of lineage-specific TFs drives genome reorganization that precedes changes in gene expression [22].

We then turned to analyze the impact of the organization of the genome under basal conditions on transcriptional programs that are induced in response to various triggers. First, we showed that both induced TF binding events and induced genes are enriched in the A compartment (**Fig. 5**), indicating that preexisting A/B compartments within a cell constrains its network of induced TF-chromatin interactions and activated genes. We then demonstrated the association between cell-type specific response to triggers and basal cell-type specific AB compartmentalization. Cell-type specific induced TF binding and activated genes show significant enrichment for cell-type specific A compartments (**Table 3 and 4**). Yet, here too, a large portion of the cell-type specific induced TFBS and genes are located in genomic regions that are assigned to the A compartment in both responsive and non-responsive cell lines, further underscoring that additional key factors participate in shaping the specific transcriptional response to challenges elicited in each cell type.

Current techniques for determining the 3D organization of the genome are still limited in their resolution and sensitivity. Further development of these methods together with advances in their application to single cells will allow us to better understand how the genome is reorganized at multiple structural layers in response to various triggers and stresses, and to elucidate how this topological reorganization is causally linked to cell-type specific transcriptional programs that are induced in response to these challenges.

Conclusions

Collectively, the large-scale meta-analysis that we carried out in this study further demonstrates the strong association between cell-type specific A/B compartmentalization, modulation of landscape of TF-chromatin interactions and differential gene expression. Moreover, our results further indicate a role for the 3D organization of the genome under basal conditions, at the layers of both A/B compartmentalization and intra-TAD enhancer-promoter interactions, in shaping TF binding events and the network of genes that are induced in response to treatment.

Methods

Identification of A and B compartments from Hi-C data. We defined A/B compartments for 13 human cell lines for which Hi-C data are available (**Supplementary Table 1**). Identification of A and B compartments was performed similarly to what has been previously described [5, 11]. Briefly, Hi-C contact frequency matrix was first normalized using the Knight and Ruiz matrix balancing method [23]. Then, we performed principal component analysis (PCA) for each intrachromosomal matrix separately. In most cases, the first principal component vector partitions the chromosome into two compartments, A and B, according to the sign of the elements. In the other cases, mostly in short chromosomes, the first principal component divides the chromosome to its two arms and the second component partition it to the A/B compartments. As seen in previous studies [7], the A compartment is gene rich and its chromatin is less dense, while the B regions are gene poor and their chromatin is denser. Thus, we determined, for each chromosome separately, whether positive or negative values of the PC that indicates the A/B compartmentalization correspond to A or B based on gene richness; the compartment with higher gene density was labeled as A compartment. Centromeric regions were not included in the A/B partitions since no chromatin interactions are identified by Hi-C in these regions.

RNA-seq analysis. RNA-seq data were analyzed using a standard pipeline. Briefly, raw sequence data were downloaded from GEO/SRA DB, and mapped to the human genome (hg19) using tophat2 [24]. The number of reads that mapped to each annotated gene was counted using HTSeq-counts [25] based on GENCODE annotations [26]. Gene expression estimates were normalized to RPKM. We compared expression profiles between treated and control samples and defined the genes whose expression was changed by at least 1.5-fold as differential genes. (To avoid inflation of lowly expressed genes among the called differential genes we used a floor level of 1.0 RPKM).

ChIP-seq analysis. To ensure analysis uniformity, we did not rely on peaks called by original studies, but downloaded raw sequence data and detected TF peaks ourselves. Briefly, for each ChIP-seq experiment, reads were aligned to the human genome (hg19) using bowtie2 [27] and peaks were called using MACS2 by comparing IP and input

samples. For detection of peaks induced upon treatment, IP samples measured under control and treated conditions were directly compared [28].

AB Density factor D. For each transcription factor and cell line we computed the *AB density factor*, D, defined as follows: Let the number of observed binding sites in region S be $O(S)$ and number of expected binding sites in region S be $E(S)$:

$$D = \frac{O(A)/O(B)}{E(A)/E(B)}$$

$D > 1$ implies that binding sites are enriched for A compartment and $D < 1$ implies that binding sites are enriched for B compartment. For TF binding sites, $E(A)/E(B)$ is equal to the ratio between the genomic size of the two compartments.

AB Occupancy enrichment ratio R. For pairwise comparisons between cells, to test if cell-type specific TFBSs occur more often in regions assigned as A compartment in the cell line where the binding event was detected and as B in the other cell line than the opposite assignment, we defined the *AB occupancy enrichment ratio* R, as follows: Let the number of BSs in region S occurring only in cell line i be $n(i, S)$. Then

$$R = \frac{n(1, AB) + n(2, BA)}{n(1, BA) + n(2, AB)}$$

Declarations

Ethics approval and consent to participate. Not applicable

Consent for publication. Not applicable

Availability of data and material. All analyses carried out in this study used publicly available datasets. References are provided in the supplementary tables.

Competing interests. The authors declare that they have no competing interests

Funding. Study supported in part by the DIP German-Israeli Project cooperation (to R.E. and R.S.) and by the Kadar Family Award of the Naomi Foundation (to R.S.).

Authors' contributions. I.N., R.S., and R.E. designed the research. I.N. performed the analyses, R.E. and R.S. critically reviewed the analyses and . wrote the manuscript. All authors approved the final version.

Acknowledgements. R.E. is a Faculty Fellow of the Edmond J. Safra Center for Bioinformatics at Tel Aviv University.

Figure legends

Figure 1. Chromosomal compartments and gene expression. A. A/B partition of chromosome 1 for different cell lines based on Hi-C data in 100kb resolution. Dark-blue and white indicate A and B compartments, respectively. Light blue indicates areas which Hi-C could not measure interactions for, e.g., centromeres. **B.** Comparison of gene expression levels in A and B compartments for each cell line. P-values (in log10) for the significance of the difference are indicated below each comparison (Wilcoxon's test). For all cell lines, genes in A compartment are significantly more highly expressed than genes in B compartment. **C.** Association between dynamic A/B compartmentalization and differential gene expression in the comparison between the GM12878 and K562 cell lines. (AB: the set of genes that are located in compartment A in GM12878 and B in K562; BA: genes located in compartment B in GM12878 and A in K562). Genes in AB have significantly higher expression in GM12878 while genes in BA have higher expression in K562 (p value calculated using Wilcoxon's test).

Figure 2. Cell-type specific TF binding vs. cell-type specific compartments. A. Relation between cell-type specific A/B partition and CTCF binding sites for six cell lines. For all pair-wise comparisons, CTCF BSs specific to cell 1 (cell 2) showed significant preference to AB (BA) genomic regions over BA (AB) regions. All p-values are highly significant (-log10, chi-square test). **B.** Relationship between cell-type specific TFBSs and A/B compartments in the comparison between GM12878 and K562. For each of the 49 TFs we calculated the *AB occupancy enrichment ratio* as a measure for the preference of its cell-type specific binding events to AB genomic regions over BA regions.

Figure 3. Gene expression levels vs. promoter interactions in compartment A. A. Genes in compartment A were partitioned into three groups according to their expression levels. For each group, the distribution of genes over bins of number of promoter interactions, inferred from Hi-C data, is shown. P-value was calculated using Wilcoxon's test comparing the distributions in the least and most abundant expression groups. **B.** Genes in compartment A were partitioned into three groups according to the number of interactions their promoters are engaged in, and the distributions of gene expression levels were compared (p-value is for Wilcoxon test comparing the group of genes with 0

interactions to the genes with at least one interaction). **C-D.** Same analysis as in B and A, respectively, but here using promoter interactions derived from RNA PolII ChIA-PET data in the GM12878 cell line.

Figure 4. Differential promoter interactions vs. differential gene expression. A. Genes located in the A compartment in both MCF7 and K562 cell lines (AA genes) were divided into four groups according to the engagement of their promoters in chromatin interactions in the two cell lines (as indicated by RNA PolII ChIA-PET data). Gene sets 00, 01, 10, and 11 correspond, respectively, to the set of genes whose promoter is engaged in chromatin interactions in either none, only K562, only MCF7 or both cell lines. Expression levels in both cell lines are plotted for each gene set. Color indicates gene density. **B**. Distribution of fold-change in gene expression (log2) between MCF7 and K562 was calculated for each gene set. Highly significant association between differential gene expression and differential involvement of promoters in chromatin interaction was observed. p-values are computed using Wilcoxon test.

Figure 5. Enrichment of treatment-induced TFBSs and genes in the basal A compartment. A. TFBSs induced by various treatments are significantly enriched in the A compartment (as determined in the cells under basal condition). Experiments are sorted by p-value, enrichment ratios are represented by bars. Red line: p-value = 0.01, orange line: enrichment ratio = 1. **B.** Same as A, but for treatment-induced genes.

Figure 6. Engagement of promoters of treatment-induced genes in basal chromatin interactions. We used permutation tests to assess the significance of the engagement in chromatin interactions observed for promoters of genes that were induced upon challenges. The figure shows the analysis for the set of genes that were induced in GM12878 cells upon TNFα treatment (the positive set). 10,000 randomly selected gene sets of the same size and with the same basal expression distribution as the positive set were used to generate a null distribution. The mean number of promoter interactions per gene (3.9) was significantly higher for the positive set.

Supplementary Figure legends

Supplementary Figure 1. **Association between changes in A/B compartmentalization and differential gene expression between cell types**. For each pair of cell lines, we examined the difference (fold-change) in expression level between genes assigned to the AB and BA sets (for a pair of cell lines 1 and 2, AB: genes located in the A compartments in cell line 1 and in B in cell line 2; BA: genes located in the B compartment in cell line 1 and in A in cell line 2). For 27 out of 28 pairwise comparisons (all except HMEC-NHEK), we observed a highly significant association (FDR<<5%) between differential compartmentalization and expression. (p-values calculated using Wilcoxon's test.)

Supplementary Figure 2. **Enrichment of TFBSs in the A compartment**. ChIP-seq experiments are sorted by p-value, A-B density factors are represented by bars. Red line indicates p-value = 0.01. Shown are experiments in the GM12878 cell line. Similar results were observed for all other cell lines (data not shown).

Supplementary Figure 3. **Gene expression levels vs. promoter interactions in compartment A**. The same analyses described in the legend of Fig. 3 are applied here to additional cell lines.

Tables

Table 1. Genomic size and number of genes assigned to A/B compartments.

Cell line	A Total size (Mbp)	# Genes in A	B Total size (Mbp)	# Genes in B
GM12878	1,322	15,184	1,410	3,958
K562	1,376	15,401	1,356	3,741
HUVEC	1,382	15,116	1,350	4,022
HMEC	1,317	14,593	1,415	4,543
NHEK	1,433	14,864	1,300	4,276
IMR90	1,310	13,569	1,423	5,577
T47D	1,372	14,114	1,350	4,979
MCF7	1,384	15,056	1,450	4,758
MCF10	1,386	15,090	1,451	4,772
LNCAP	1,433	14,112	1,299	5,021
PC3	1,395	13,341	1,313	5,692
KBM7	1,301	14,506	1,431	4,631
PrEC	1,327	13,994	1,387	5,041

Table 2. Comparison of binding site and epigenetic mark occupancy in A/B compartments between two cell types

A. CTCF

HMEC-HUVEC	AA	AB	BA	BB	total	R	p-value
HMEC only CTCF BSs	7,241	**1,655**	947	4,775	14,618	2.34	10^{-168}
HUVEC only CTCF BSs	4,516	264	**1,180**	1,524	7,484		
Common CTCF BSs	24,986	2,587	4,647	9,750	41,970		

B. H3K9ac

GM12878 - NHEK	AA	AB	BA	BB	total	R	p-value
GM12878 only H3K9ac peaks	14,695	**3,111**	596	1,708	20,110	4.54	$<10^{-300}$
NHEK only H3K9ac peaks	19,997	1,401	**5,949**	4,154	31,501		
Common H3K9ac peaks	21,594	2,036	1,078	2,911	27,619		

C. H3K27me3

MCF7-GM12878	AA	AB	BA	BB	total	R	p-value
MCF7 only H3K27me3 peaks	5,213	1,751	**3,637**	9,712	20,313	0.54	10^{-122}
GM12878 only H3K27me3 peaks	7,176	**1,765**	1,145	3,608	13,694		
Common H3K27me3 peaks	318	95	118	317	848		

Table 3. Cell-type specific treatment-induced TFBSs show preference to cell-type specific A compartment.

MCF7 - T47D; Treatment: Estradiol Antibody: ER	AA	AB	BA	BB	total	A/B Enrichment	R	p-value
MCF7 only ESR1 BSs	9,656	**2,356**	1,459	3,285	16,756	1.61	1.61	3.29E-29
T47D only ESR1 BSs	2,031	257	**410**	475	3,173	1.6		
Common ESR1 BSs	3,138	406	330	461	4,335			

Table 4. Cell-type specific treatment-induced genes show preference to cell-type specific basal A compartment.

HMEC - MCF7	AA	AB	BA	BB	Total	R	Enrichment	p-value
Induced only in HMEC	29	**20**	6	9	64	3.44	2.0	0.00095
Induced only in MCF7	267	22	**36**	33	358	1.67		
induced in both	34	4	1	4	43			

References

1. Dekker J, Marti-Renom MA, Mirny LA: **Exploring the three-dimensional organization of genomes: interpreting chromatin interaction data.** *Nat Rev Genet* 2013, **14:**390-403.
2. Sexton T, Cavalli G: **The role of chromosome domains in shaping the functional genome.** *Cell* 2015, **160:**1049-1059.
3. Schmitt AD, Hu M, Ren B: **Genome-wide mapping and analysis of chromosome architecture.** *Nat Rev Mol Cell Biol* 2016, **17:**743-755.
4. Gibcus JH, Dekker J: **The hierarchy of the 3D genome.** *Mol Cell* 2013, **49:**773-782.
5. Barutcu AR, Lajoie BR, McCord RP, Tye CE, Hong D, Messier TL, Browne G, van Wijnen AJ, Lian JB, Stein JL, et al: **Chromatin interaction analysis reveals changes in small chromosome and telomere clustering between epithelial and breast cancer cells.** *Genome Biol* 2015, **16:**214.
6. Cremer T, Cremer M, Dietzel S, Muller S, Solovei I, Fakan S: **Chromosome territories--a functional nuclear landscape.** *Curr Opin Cell Biol* 2006, **18:**307-316.
7. Lieberman-Aiden E, van Berkum NL, Williams L, Imakaev M, Ragoczy T, Telling A, Amit I, Lajoie BR, Sabo PJ, Dorschner MO, et al: **Comprehensive mapping of long-range interactions reveals folding principles of the human genome.** *Science* 2009, **326:**289-293.
8. Dixon JR, Gorkin DU, Ren B: **Chromatin Domains: The Unit of Chromosome Organization.** *Mol Cell* 2016, **62:**668-680.
9. Nora EP, Lajoie BR, Schulz EG, Giorgetti L, Okamoto I, Servant N, Piolot T, van Berkum NL, Meisig J, Sedat J, et al: **Spatial partitioning of the regulatory landscape of the X-inactivation centre.** *Nature* 2012, **485:**381-385.
10. Dixon JR, Selvaraj S, Yue F, Kim A, Li Y, Shen Y, Hu M, Liu JS, Ren B: **Topological domains in mammalian genomes identified by analysis of chromatin interactions.** *Nature* 2012, **485:**376-380.
11. Dixon JR, Jung I, Selvaraj S, Shen Y, Antosiewicz-Bourget JE, Lee AY, Ye Z, Kim A, Rajagopal N, Xie W, et al: **Chromatin architecture reorganization during stem cell differentiation.** *Nature* 2015, **518:**331-336.
12. Le Dily F, Bau D, Pohl A, Vicent GP, Serra F, Soronellas D, Castellano G, Wright RH, Ballare C, Filion G, et al: **Distinct structural transitions of chromatin topological domains correlate with coordinated hormone-induced gene regulation.** *Genes Dev* 2014, **28:**2151-2162.
13. Smallwood A, Ren B: **Genome organization and long-range regulation of gene expression by enhancers.** *Curr Opin Cell Biol* 2013, **25:**387-394.
14. Schoenfelder S, Clay I, Fraser P: **The transcriptional interactome: gene expression in 3D.** *Curr Opin Genet Dev* 2010, **20:**127-133.
15. Jin F, Li Y, Dixon JR, Selvaraj S, Ye Z, Lee AY, Yen CA, Schmitt AD, Espinoza CA, Ren B: **A high-resolution map of the three-dimensional chromatin interactome in human cells.** *Nature* 2013, **503:**290-294.
16. Ron G, Globerson Y, Moran D, Kaplan T: **Promoter-enhancer interactions identified from Hi-C data using probabilistic models and hierarchical topological domains.** *Nat Commun* 2017, **8:**2237.
17. Niepel M, Hafner M, Duan Q, Wang Z, Paull EO, Chung M, Lu X, Stuart JM, Golub TR, Subramanian A, et al: **Common and cell-type specific responses to anti-cancer drugs revealed by high throughput transcript profiling.** *Nat Commun* 2017, **8:**1186.

18. Troester MA, Hoadley KA, Sorlie T, Herbert BS, Borresen-Dale AL, Lonning PE, Shay JW, Kaufmann WK, Perou CM: **Cell-type-specific responses to chemotherapeutics in breast cancer.** *Cancer Res* 2004, **64:**4218-4226.
19. Rashi-Elkeles S, Elkon R, Shavit S, Lerenthal Y, Linhart C, Kupershtein A, Amariglio N, Rechavi G, Shamir R, Shiloh Y: **Transcriptional modulation induced by ionizing radiation: p53 remains a central player.** *Mol Oncol* 2011, **5:**336-348.
20. Mullen AC, Orlando DA, Newman JJ, Loven J, Kumar RM, Bilodeau S, Reddy J, Guenther MG, DeKoter RP, Young RA: **Master transcription factors determine cell-type-specific responses to TGF-beta signaling.** *Cell* 2011, **147:**565-576.
21. Heinz S, Romanoski CE, Benner C, Glass CK: **The selection and function of cell type-specific enhancers.** *Nat Rev Mol Cell Biol* 2015, **16:**144-154.
22. Stadhouders R, Vidal E, Serra F, Di Stefano B, Le Dily F, Quilez J, Gomez A, Collombet S, Berenguer C, Cuartero Y, et al: **Transcription factors orchestrate dynamic interplay between genome topology and gene regulation during cell reprogramming.** *Nat Genet* 2018, **50:**238-249.
23. Rao SS, Huntley MH, Durand NC, Stamenova EK, Bochkov ID, Robinson JT, Sanborn AL, Machol I, Omer AD, Lander ES, Aiden EL: **A 3D map of the human genome at kilobase resolution reveals principles of chromatin looping.** *Cell* 2014, **159:**1665-1680.
24. Kim D, Pertea G, Trapnell C, Pimentel H, Kelley R, Salzberg SL: **TopHat2: accurate alignment of transcriptomes in the presence of insertions, deletions and gene fusions.** *Genome Biol* 2013, **14:**R36.
25. Anders S, Pyl PT, Huber W: **HTSeq--a Python framework to work with high-throughput sequencing data.** *Bioinformatics* 2015, **31:**166-169.
26. Harrow J, Frankish A, Gonzalez JM, Tapanari E, Diekhans M, Kokocinski F, Aken BL, Barrell D, Zadissa A, Searle S, et al: **GENCODE: the reference human genome annotation for The ENCODE Project.** *Genome Res* 2012, **22:**1760-1774.
27. Langmead B, Salzberg SL: **Fast gapped-read alignment with Bowtie 2.** *Nat Methods* 2012, **9:**357-359.
28. Liu T: **Use model-based Analysis of ChIP-Seq (MACS) to analyze short reads generated by sequencing protein-DNA interactions in embryonic stem cells.** *Methods Mol Biol* 2014, **1150:**81-95.

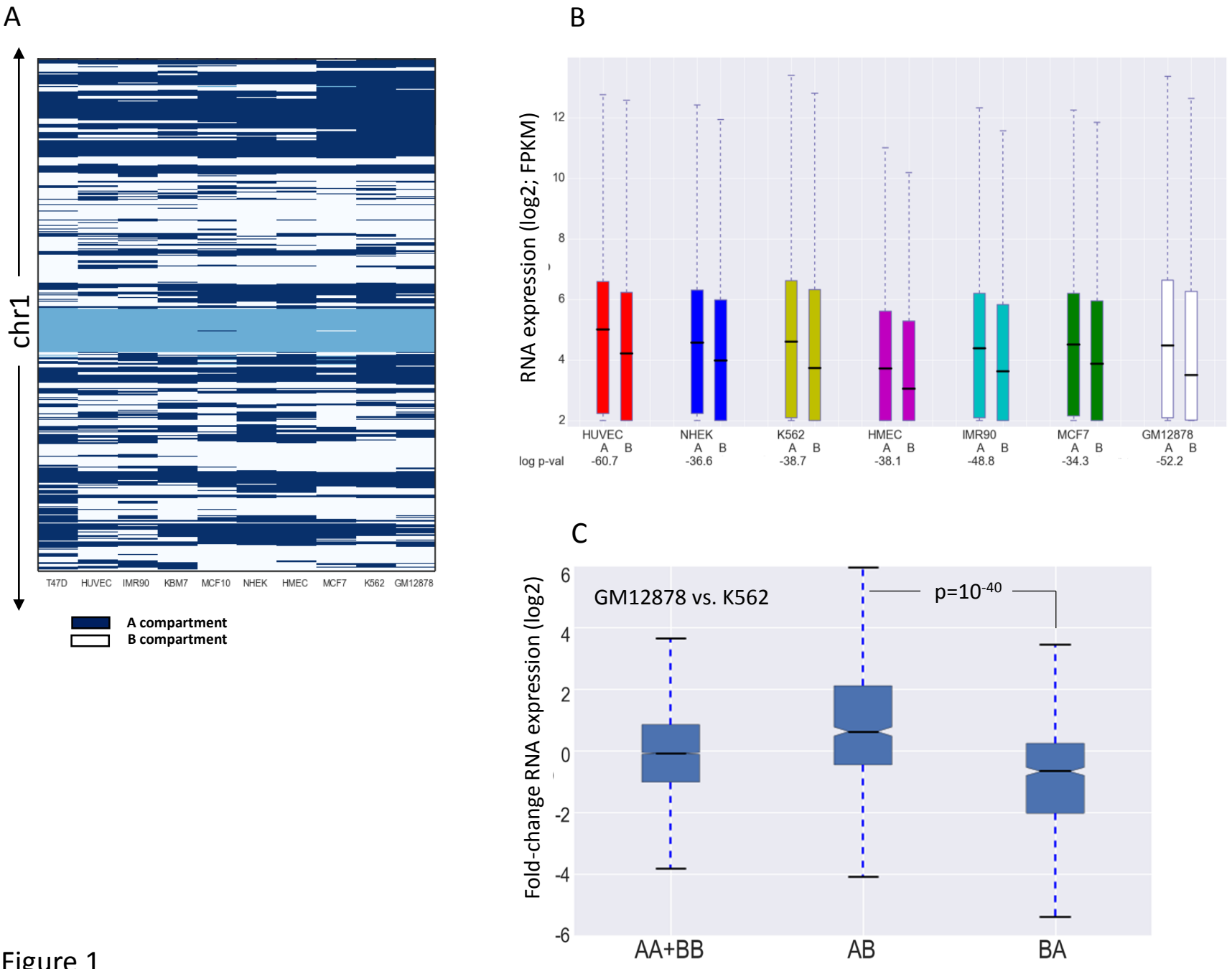
A
chr1
T47D HUVEC IMR90 KBM7 MCF10 NHEK HMEC MCF7 K562 GM12878
A compartment
B compartment
B
RNA expression (log2; FPKM)
12
10
8
6
4
2
HUVEC NHEK K562 HMEC IMR90 MCF7 GM12878
A B A B A B A B A B A B A B
log p-val -60.7 -36.6 -38.7 -38.1 -48.8 -34.3 -52.2
C
GM12878 vs. K562
p=10-40
Fold-change RNA expression (log2)
6
4
2
0
-2
-4
-6
AA+BB
AB
BA

Figure 1

A

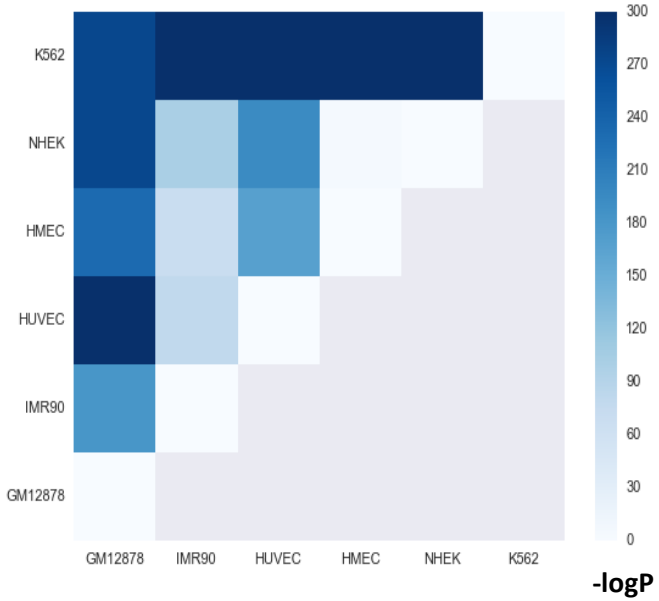

Prefernce of cell-type specific CTCF binding to cell-type specific A compartments

B

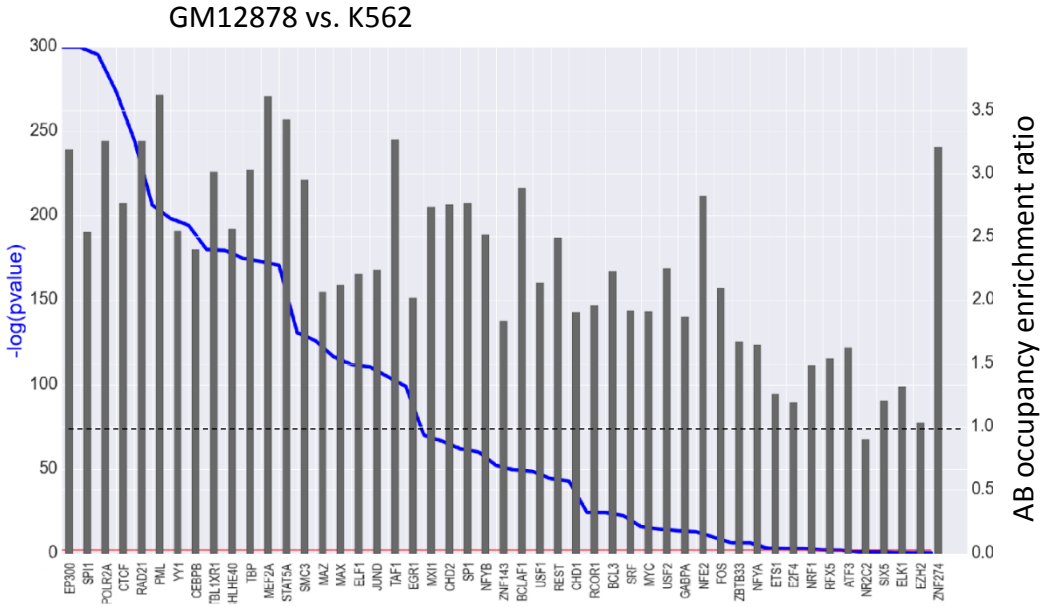

Figure 2

A

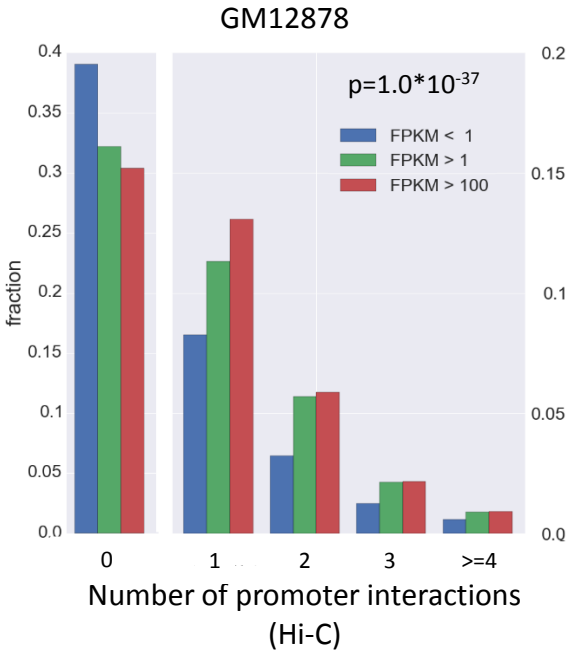

B

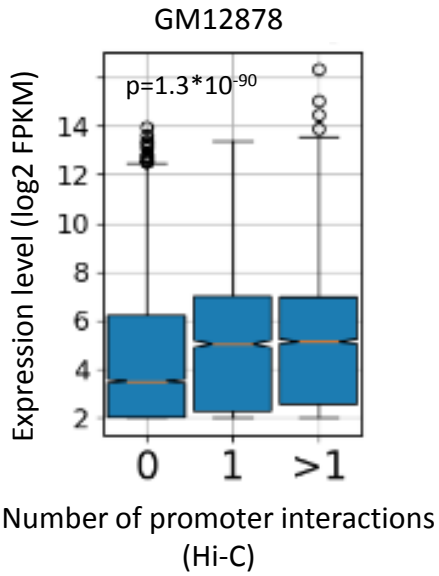

D

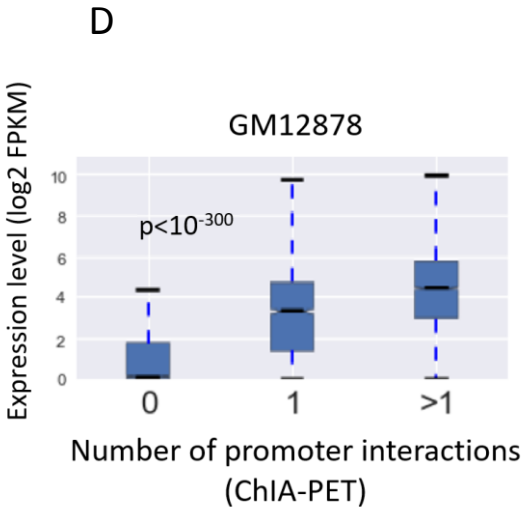

C

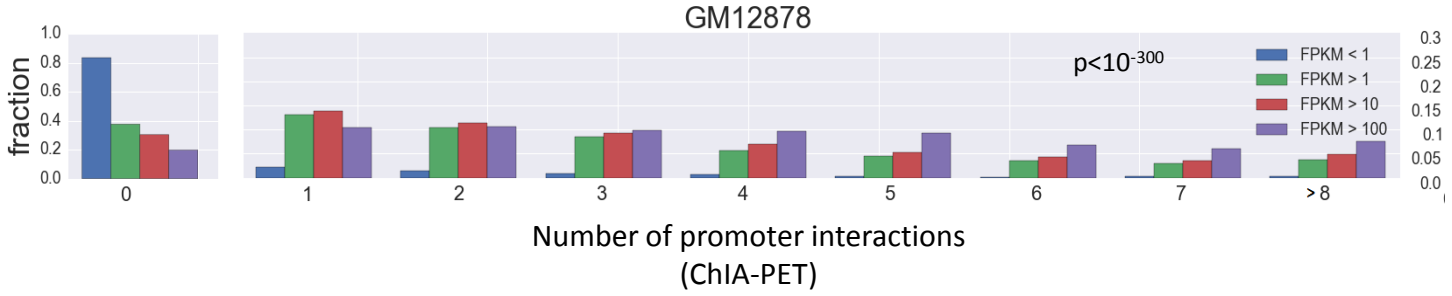

Figure 3

A

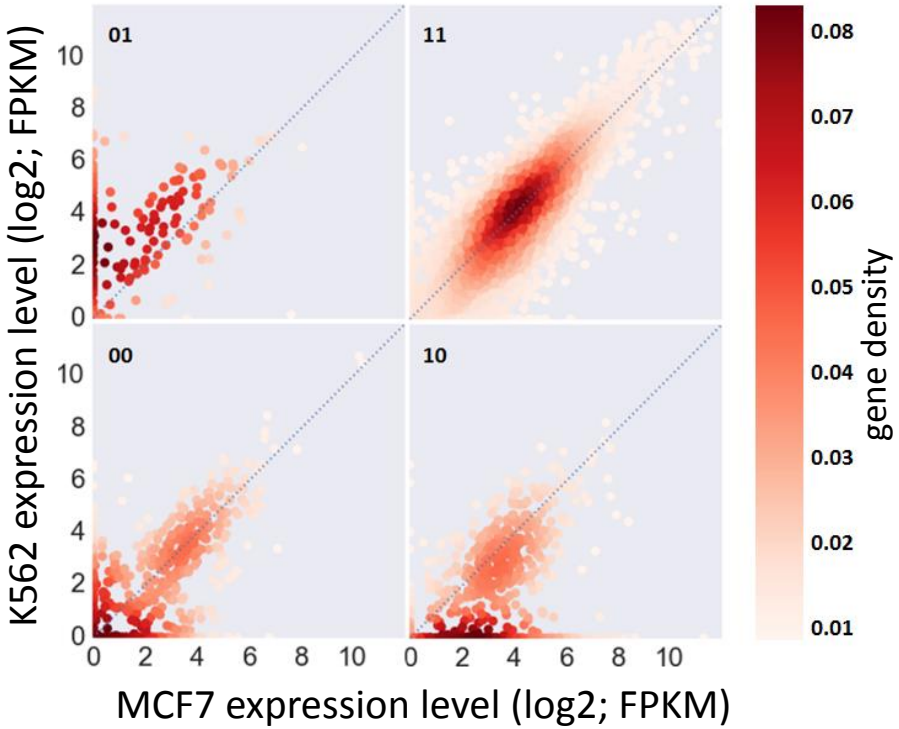
01
11
00
10
K562 expression level (log2; FPKM)
MCF7 expression level (log2; FPKM)
gene density
0.08
0.07
0.06
0.05
0.04
0.03
0.02
0.01

B

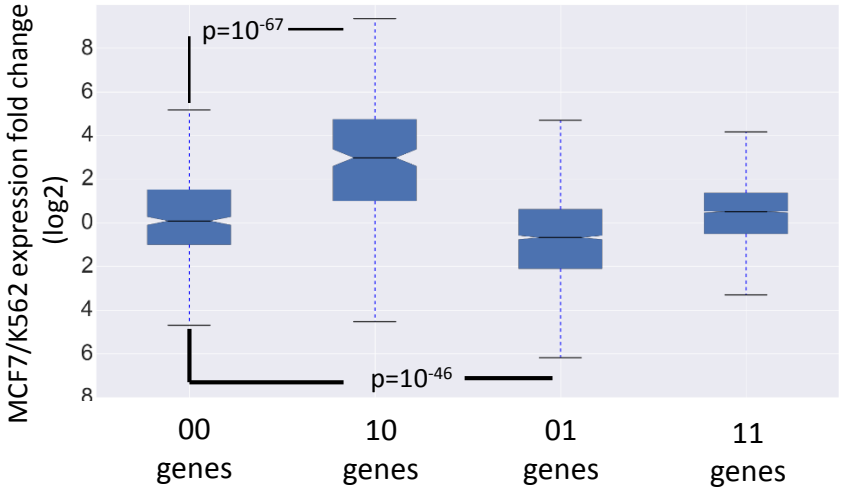
MCF7/K562 expression fold change (log2)
p=10-67
p=10-46
00 genes
10 genes
01 genes
11 genes

Figure 4

A

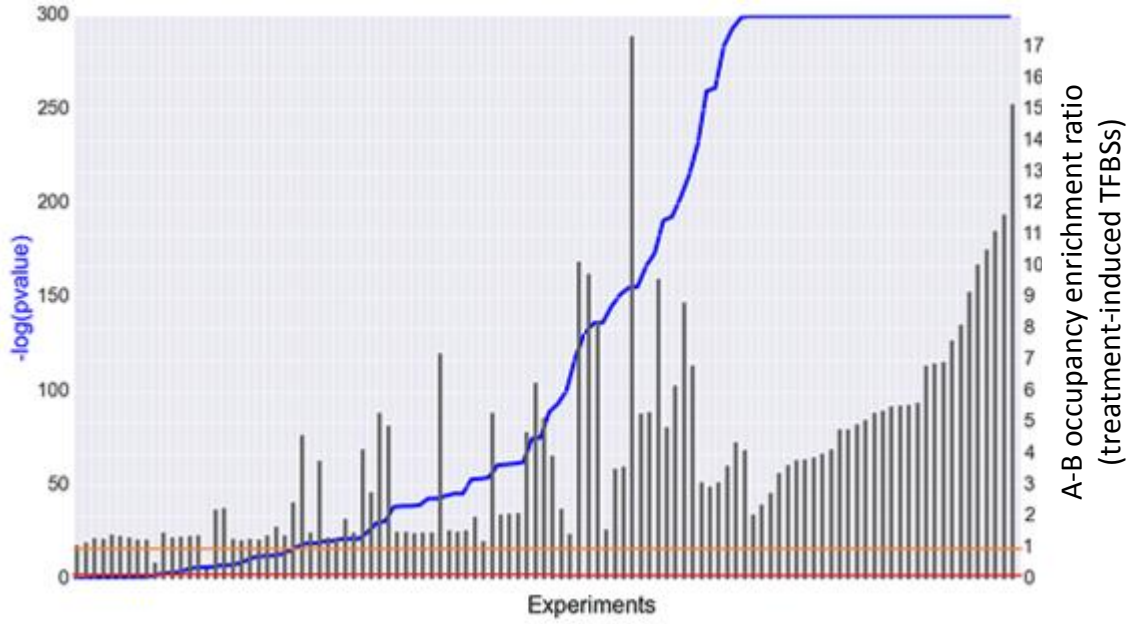
-log(pvalue)
A-B occupancy enrichment ratio
(treatment-induced TFBSs)
Experiments

B

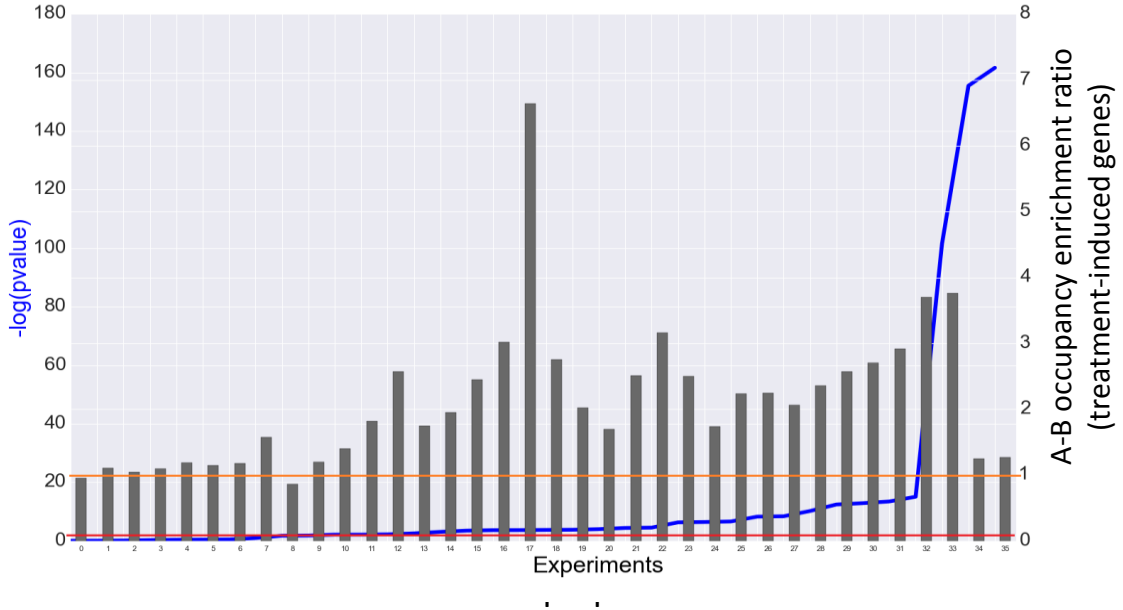
-log(pvalue)
A-B occupancy enrichment ratio
(treatment-induced genes)
Experiments

Figure 5

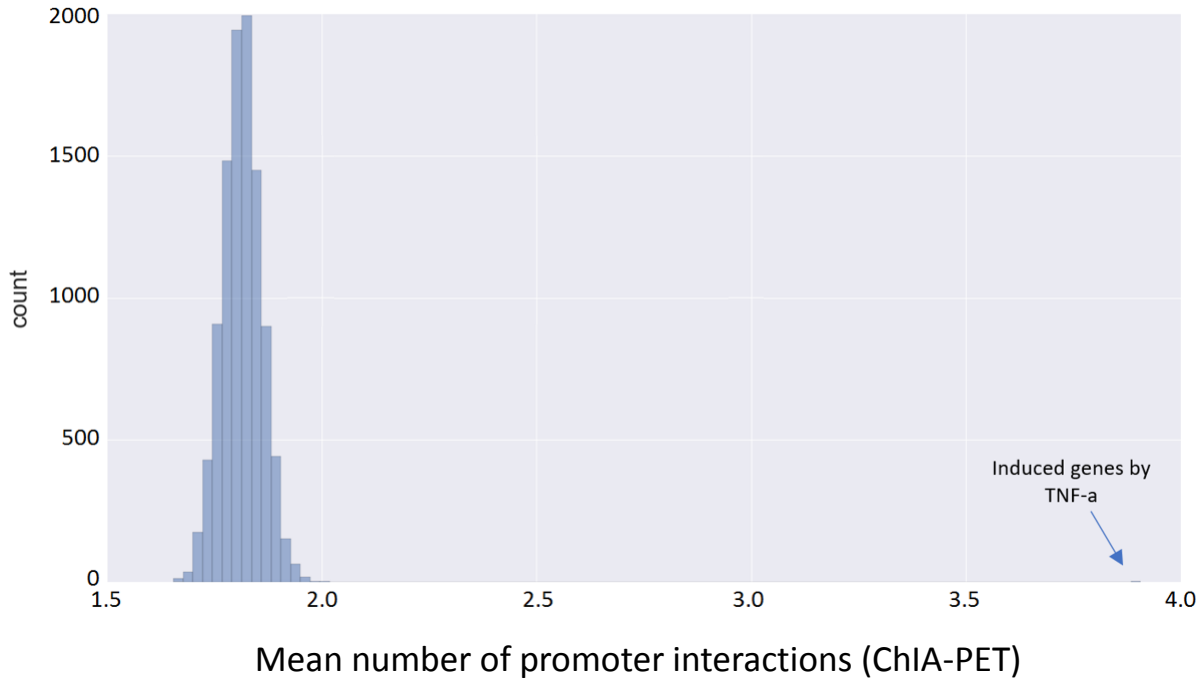
2000
1500
1000
500
0
count
1.5
2.0
2.5
3.0
3.5
4.0
Induced genes by
TNF-a
Mean number of promoter interactions (ChIA-PET)

Figure 6

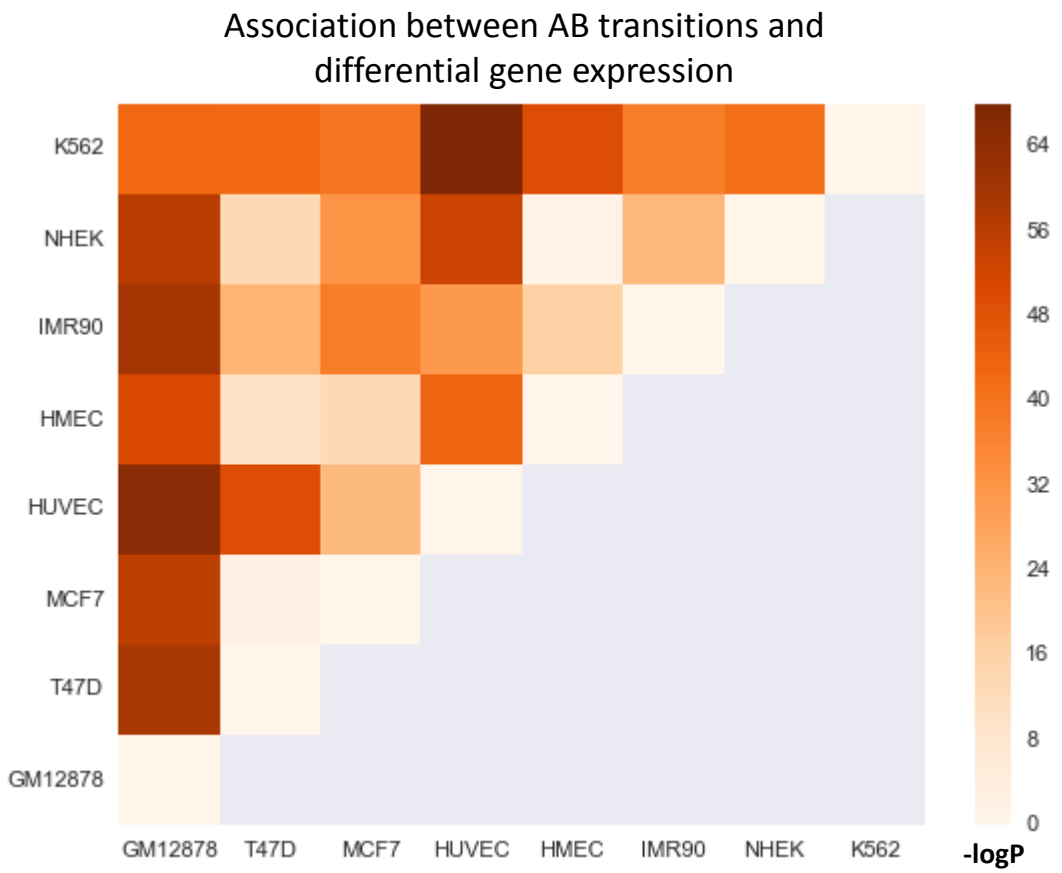

Supplementary Figure 1

GM12878 – TF enrichment for A compartment

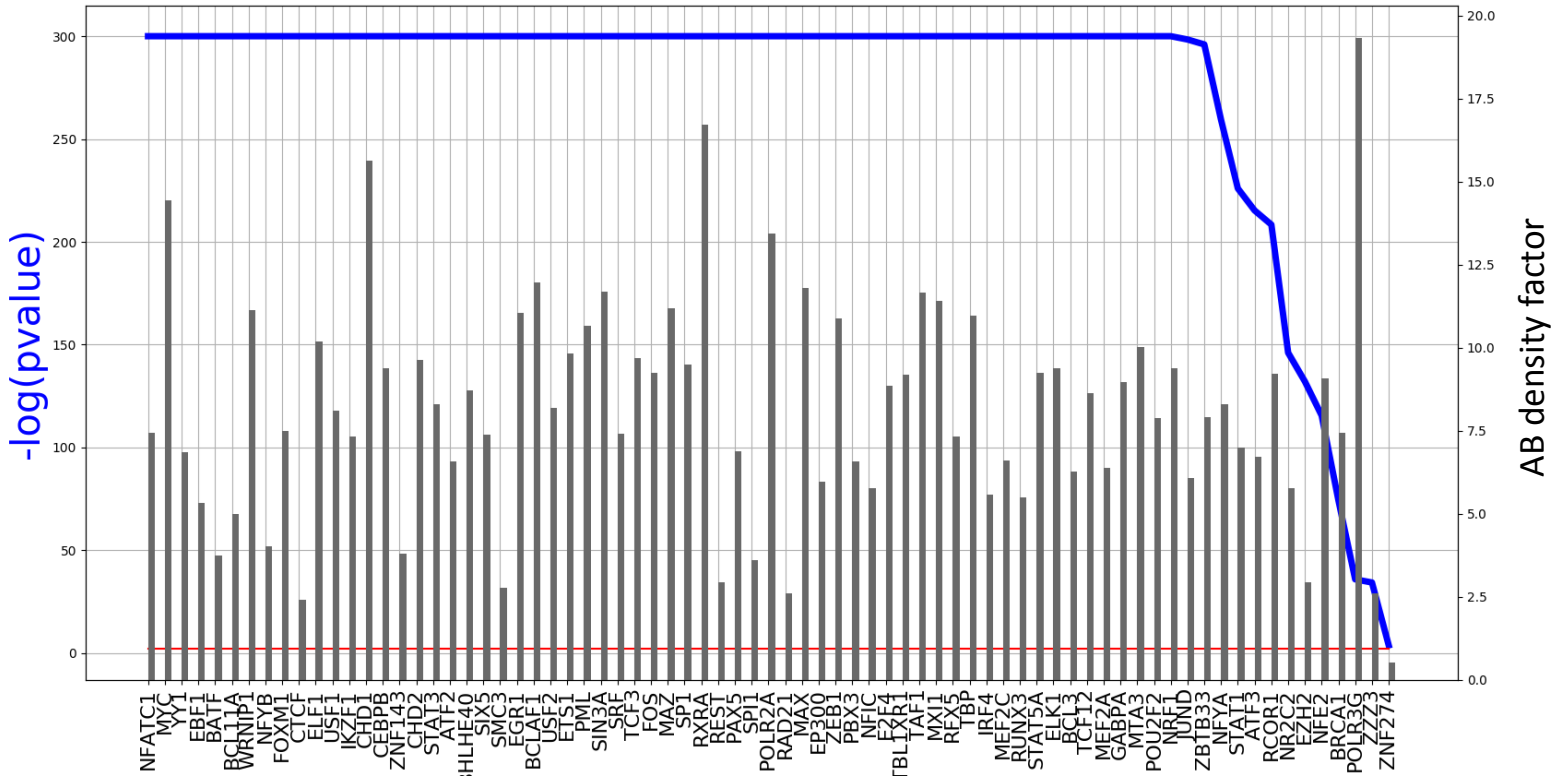

Supplementary Figure 2

A

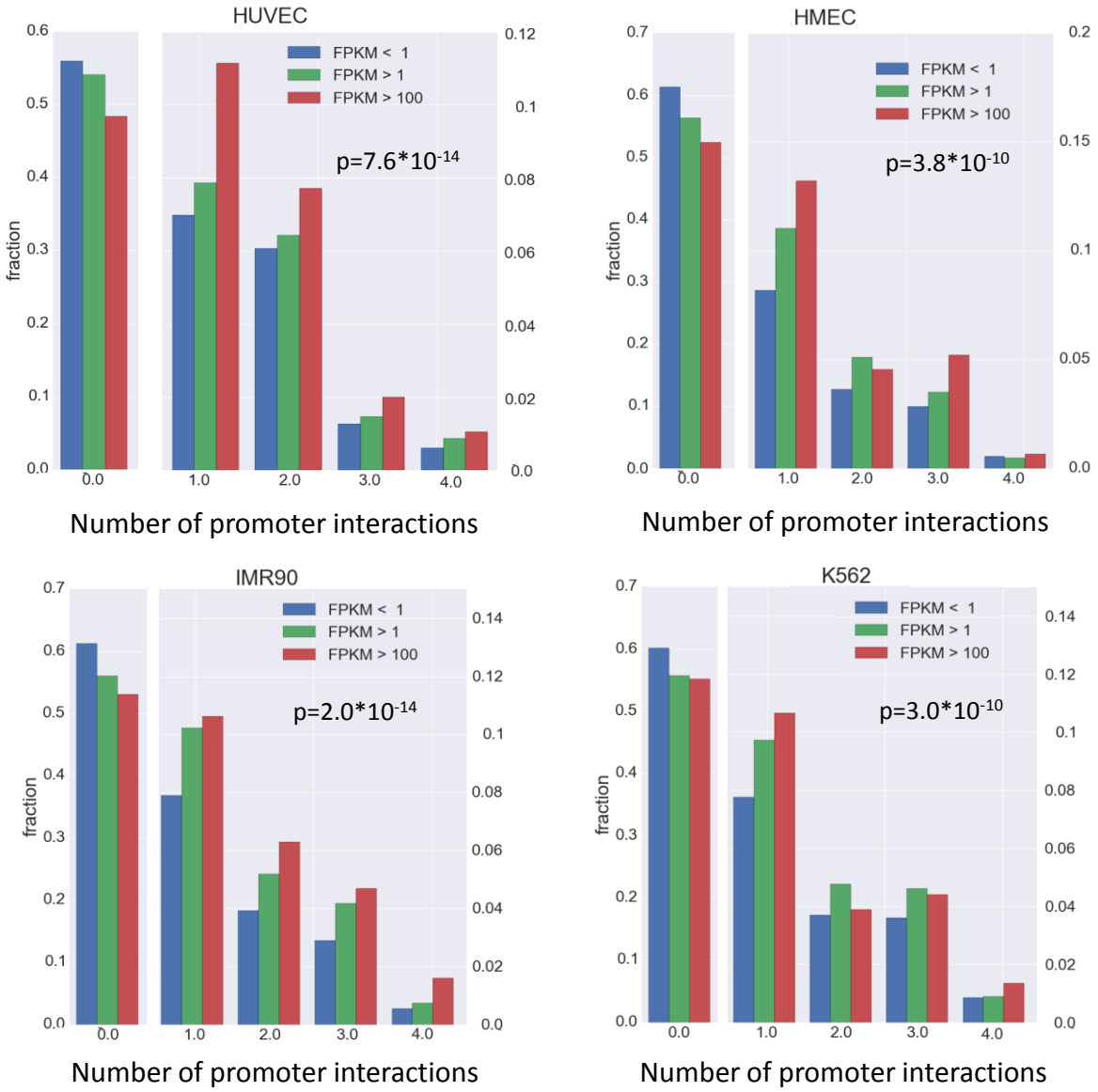

Supplementary Figure 3

B

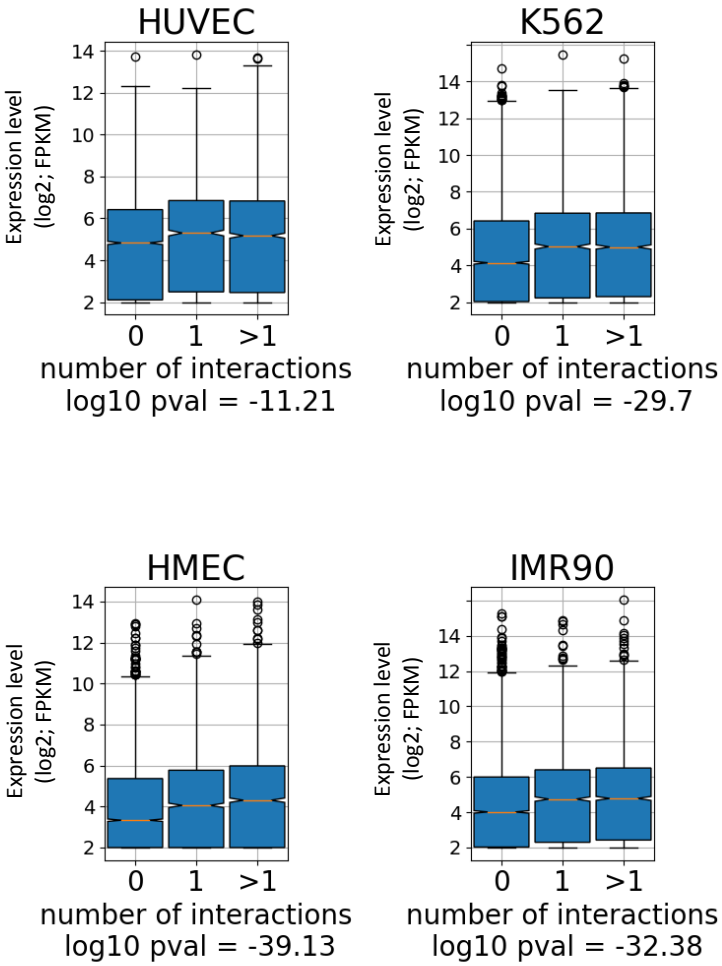

Supplementary Figure 3

C

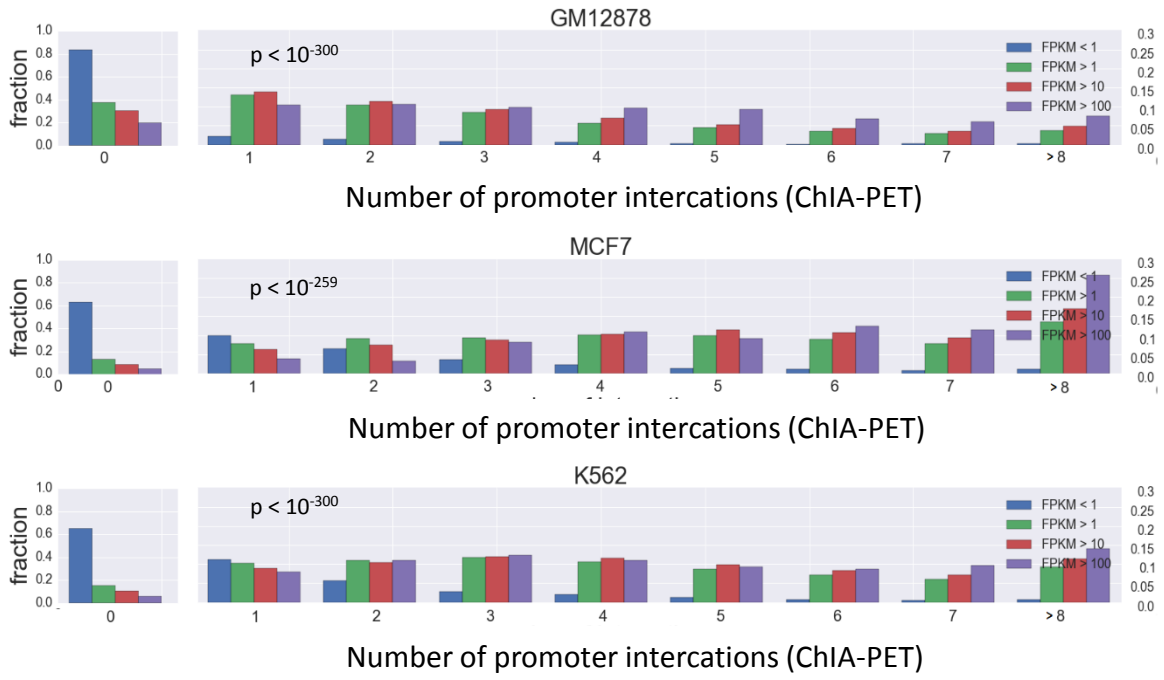

D

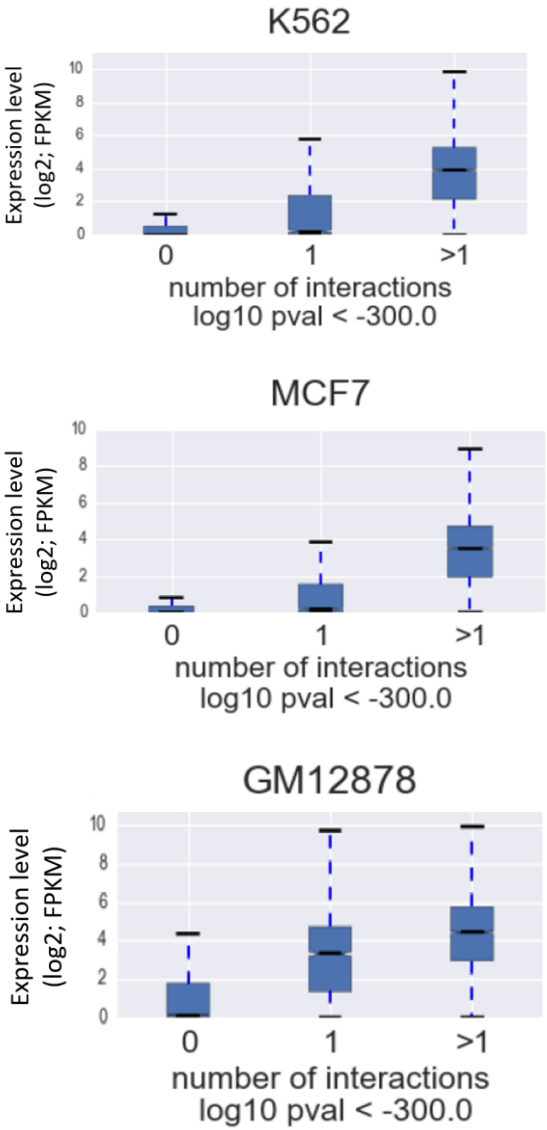

Supplementary Figure 3

Supplementary Table 1. Hi-C datasets

Cell line	Description	Hi-C data resolution (Kbp)	Source study
MCF10A	Non-tumorigenic epithelial breast cell line	40, 250	[1]
MCF7	Breast cancer cell line with overexpression of estrogen receptor		
LNCAP	Androgen sensitive prostate adenocarcinoma cell line	40, 100	[2]
PrEC	Prostate epithelial cell line	40	
PC3	Androgen insensitive prostate cancer cell line		
HUVEC	Human umbilical vein endothelial cell line	5, 10, 100, 250, 500, 1000	[3]
NHEK	Primary normal human epidermal keratinocytes cell line		
IMR90	Fetal lung fibroblasts cell line		
K562	Myelogenous leukemia cell line		
KBM7	Chronic myelogenous leukemia cell line		
HMEC	Human mammary epithelial cell line		
GM12878	Lymphoblastoid cell line	1, 5, 10, 100, 250, 500, 1000	
T47D	Breast cancer cell line	100	[4]

Supplementary Table 2. ENCODE ChIP-seq data included in our analyses (122 TFs profiled in cell lines with Hi-C data)

Transcription factor	Cell lines with available ChIP-Seq dataset in ENCODE
ZBTB33	K562, GM12878
CTCF	K562, HUVEC, NHEK, HMEC, IMR90, GM12878
EGR1	K562, GM12878
RUNX3	GM12878
MAZ	K562, GM12878
RAD21	K562, GM12878, IMR90
SMC3	K562, GM12878
MAFK	K562, IMR90
MAFF	K562
E2F6	K562
MAX	K562, GM12878, HUVEC
PAX5	GM12878
POLR2A	K562, HUVEC, GM12878, IMR90, NHEK
PHF8	K562
PML	K562, GM12878
YY1	K562, GM12878
TAF1	K562, GM12878
SIN3AK20	K562
GTF2F1	K562
ATF2	GM12878
MYC	K562, GM12878, HUVEC
MXI1	GM12878, K562
JUND	K562, GM12878
POU2F2	GM12878
KDM5B	K562
TBP	K562, GM12878
EP300	K562, GM12878

ELK1	GM12878, K562
RFX5	K562, GM12878
CHD2	K562, GM12878
ATF3	K562, GM12878
BRCA1	GM12878
NFYA	K562, GM12878
NFYB	K562, GM12878
JUN	K562, HUVEC
GABPA	K562, GM12878
E2F4	K562, GM12878
SP1	K562, GM12878
SRF	K562, GM12878
ELF1	K562, GM12878
USF1	K562, GM12878
ATF1	K562
SIX5	K562, GM12878
USF2	GM12878, K562
FOS	K562, HUVEC, GM12878
TBL1XR1	K562, GM12878
ZNF143	K562, GM12878
SP2	K562
EBF1	GM12878
CTCFL	K562
TEAD4	K562
THAP1	K562
ZEB1	GM12878
CEBPB	K562, IMR90, GM12878
PBX3	GM12878
UBTF	K562
CBX3	K562
BCLAF1	K562, GM12878

RBBP5	K562
RCOR1	K562, GM12878
FOSL1	K562
GATA2	K562, HUVEC
BHLHE40	K562, GM12878
TAL1	K562
BCL3	GM12878, K562
NFATC1	GM12878
MEF2A	GM12878, K562
MEF2C	GM12878
ZNF263	K562
CCNT2	K562
HDAC2	K562
TCF3	GM12878
TCF12	GM12878
ZNF274	K562, GM12878
STAT1	GM12878
BATF	GM12878
HMGN3	K562
SETDB1	K562
TAF7	K562
SPI1	K562, GM12878
ETS1	K562, GM12878
REST	K562, GM12878
ZBTB7A	K562
EZH2	NHEK, HMEC, K562, HUVEC, GM12878
JUNB	K562
NR2F2	K562
TRIM28	K562
GTF3C2	K562
SAP30	K562

CHD1	K562, GM12878
STAT5A	K562, GM12878
HDAC1	K562
NRF1	K562, GM12878
NR2C2	GM12878, K562
SIN3A	GM12878
GATA1	K562
NFIC	GM12878
IRF4	GM12878
BCL11A	GM12878
MTA3	GM12878
FOXM1	GM12878
RXRA	GM12878
KAP1	K562
BACH1	K562
HDAC8	K562
NFE2	K562, GM12878
ARID3A	K562
WRNIP1	GM12878
GTF2B	K562
HDAC6	K562
SMARCA4	K562
BRF2	K562
IKZF1	GM12878
SMARCB1	K562
STAT3	GM12878
BDP1	K562
RPC155	K562
SIRT6	K562
RDBP	K562
ZZZ3	GM12878

POLR3G	K562, GM12878
BRF1	K562

Supplementary Table 3. Enrichment of CTCF binding sites for the A compartmentalization.

Cell line	Observed A	Observed B	total	Expected A	Expected B	D	-log 10 p-value
K562	48,141	15,524	63,665	32,056	31,599	3.06	> 300
HUVEC	35,329	12,544	47,873	24,216	23,656	2.75	> 300
NHEK	45,665	16,701	62,366	32,700	29,665	2.48	> 300
HMEC	36,469	18,135	54,604	26,322	28,281	2.16	> 300
IMR90	29,184	14,880	44,064	21,121	22,942	2.13	> 300
GM12878	42,295	17,575	59,870	28,970	30,899	2.57	> 300

Supplementary Table 4A. Common and cell-type specific H3K9ac sites in the comparison between GM12878 and NHEK cell lines

	AA	AB	BA	BB	total	R	-log10 p-value
HMEC vs. GM12878							
BSs only in Cell1	17789	**6309**	1708	5087	30893	4.48	> 300
BSs only in Cell2	15292	567	**3880**	1779	21518		
Common BSs	21558	1201	2319	3613	28691		
HUVEC vs. GM12878							
BSs only in Cell1	16635	**6747**	651	3805	27838	7.64	> 300
BSs only in Cell2	16046	612	**2900**	1844	21402		
Common BSs	20606	1173	966	2614	25359		
HUVEC vs. HMEC							
BSs only in Cell1	14992	**4292**	468	3168	22920	4.16	> 300
BSs only in Cell2	16370	1369	**3341**	4301	25381		
Common BSs	27220	2629	984	4031	34864		
K562 vs. GM12878							
BSs only in Cell1	21793	**4294**	1019	3916	31022	4.56	> 300
BSs only in Cell2	14158	580	**2994**	1849	19581		
Common BSs	24463	1239	1350	2762	29814		
K562 vs. HMEC							
BSs only in Cell1	21915	**5083**	982	3672	31652	4.15	> 300
BSs only in Cell2	17015	1667	**5907**	5110	29699		
Common BSs	23268	2498	1285	3435	30486		
K562 vs. HUVEC							
BSs only in Cell1	22645	**3551**	1140	3770	31106	5.37	> 300
BSs only in Cell2	15827	627	**5944**	3772	26170		
Common BSs	22627	1193	1300	2594	27714		
NHEK vs. GM12878							
BSs only in Cell1	19997	**5949**	1401	4154	31501	4.54	> 300
BSs only in Cell2	14695	596	**3111**	1708	20110		
Common BSs	21362	1192	2042	3023	27619		
NHEK vs. HMEC							
BSs only in Cell1	11680	**1082**	471	2402	15635	1.52	26
BSs only in Cell2	7559	688	*678*	2879	11804		
Common BSs	42741	2511	2267	7437	54956		
NHEK vs. HUVEC							
BSs only in Cell1	18223	**3364**	1152	3363	26102	3.91	> 300
BSs only in Cell2	14273	584	**3426**	3056	21339		
Common BSs	26132	1241	2646	3560	33579		
NHEK vs. K562							
BSs only in Cell1	18782	**5447**	1599	3903	29731	3.46	> 300
BSs only in Cell2	21127	1132	**3998**	3561	29818		
Common BSs	23818	1357	2117	3026	30318		

Supplementary Table 4B. Common and cell-type specific H3K27me3 sites in the comparison between GM12878 and NHEK cell lines

	AA	AB	BA	BB	total	R	p-value
GM12878 vs. NHEK							
BSs only in Cell1	7244	1099	**2136**	3306	13785	0.73	1.16E-18
BSs only in Cell2	4369	*1026*	1215	3272	9882		
Common BSs	350	71	62	288	771		
GM12878 vs. K562							
MCF7 NHEK							
BSs only in Cell1	5682	1460	**4114**	9381	20637	0.45	8.56E-113
BSs only in Cell2	4902	**1066**	904	3355	10227		
Common BSs	129	64	55	168	416		
MCF7 vs. GM12878							
BSs only in Cell1	5213	1751	**3637**	9712	20313	0.54	2.04E-122
BSs only in Cell2	7176	**1765**	1145	3608	13694		
Common BSs	318	95	118	317	848		

Supplementary Table 5. Preference of induced TF binding sites and epigenetic marks to the A compartment

Cell line	treatment	antibody	induced in A	induced in B	log p-value	source
IMR90	TNF-a (10ng/mL) 1hr	p300	312	113	-25.05	[5]
IMR90	TNF-a (10ng/mL) 1hr	H3K4me3	487	104	-62.27	
IMR90	TNF-a (10ng/mL) 1hr	H3K36me3 (Abcam ab9050)	170	45	-19.06	
IMR90	TNF-a (10ng/mL) 1hr	PolII (Santa Cruz sc-899)	7613	1837	-300	
IMR90	TNF-a (10ng/mL) 1hr	flavopiridol (1ÂµM, 1hr)	9154	1655	-300	
HUVEC	TNF-a (10ng/mL) 1hr	H3K27ac (Abcam, ab4729)	5711	490	-300	
LNCAP	DHT (100nM, 2h) + TNF-alpha (1000U/ml, 2h)	anti-AR	4380	2816	-45.48	[6]
LNCAP	DHT (100nM, 2h) + TNF-alpha (1000U/ml, 2h)	anti-AR	4277	2751	-44.34	
LNCAP	DHT (100nM, 2h) + TNF-alpha (1000U/ml, 2h)	anti-AR	4611	3084	-38.47	
LNCAP	DHT (100nM, 2h) + TNF-alpha (1000U/ml, 2h)	anti-AR	4437	2943	-38.89	
LNCAP	DHT (100nM, 2h)	anti-AR	5301	3527	-45.45	
LNCAP	DHT (100nM, 2h)	anti-AR	5223	3550	-39.4	
LNCAP	DHT (100nM, 2h)	anti-AR	5475	3698	-42.89	
LNCAP	DHT (100nM, 2h)	anti-AR	5356	3662	-38.9	

LNCAP	DHT (100nM, 2h) + TNF-alpha (1000U/ml, 2h)	anti-FOXA1	4197	3270	-10.03	
LNCAP	DHT (100nM, 2h) + TNF-alpha (1000U/ml, 2h)	anti-FOXA1	3623	2858	-7.52	
LNCAP	DHT (100nM, 2h) + TNF-alpha (1000U/ml, 2h)	anti-FOXA1	6278	4755	-19.99	
LNCAP	DHT (100nM, 2h) + TNF-alpha (1000U/ml, 2h)	anti-FOXA1	6011	4524	-20.43	
LNCAP	DHT (100nM, 2h)	anti-FOXA1	181	157	-0.16	
LNCAP	DHT (100nM, 2h)	anti-FOXA1	146	138	-0.14	
LNCAP	DHT (100nM, 2h)	anti-FOXA1	6789	5540	-8.14	
LNCAP	DHT (100nM, 2h)	anti-FOXA1	6760	5385	-11.76	
LNCAP	TNF-alpha (1000 U/ml, 2h)	anti-FOXA1	222	168	-1.1	
LNCAP	TNF-alpha (1000 U/ml, 2h)	anti-FOXA1	189	147	-0.78	
LNCAP	TNF-alpha (1000 U/ml, 2h)	anti-FOXA1	506	404	-1.23	
LNCAP	TNF-alpha (1000 U/ml, 2h)	anti-FOXA1	502	402	-1.18	
LNCAP	DHT (100nM, 2h) + TNF-alpha (1000U/ml, 2h)	anti-PIAS3+PIAS1+PIAS2	2444	1751	-13.24	
LNCAP	DHT (100nM, 2h) + TNF-alpha (1000U/ml, 2h)	anti-PIAS3+PIAS1+PIAS2	2419	1749	-12.23	
LNCAP	DHT (100nM, 2h) + TNF-alpha (1000U/ml, 2h)	anti-PIAS3+PIAS1+PIAS2	832	622	-3.54	
LNCAP	DHT (100nM, 2h) + TNF-alpha (1000U/ml, 2h)	anti-PIAS3+PIAS1+PIAS2	843	637	-3.27	

LNCAP	DHT (100nM, 2h)	anti-PIAS3+PIAS1+PIAS2	1061	763	-5.96	
LNCAP	DHT (100nM, 2h)	anti-PIAS3+PIAS1+PIAS2	1022	751	-4.89	
LNCAP	DHT (100nM, 2h)	anti-PIAS3+PIAS1+PIAS2	2556	1713	-21.48	
LNCAP	DHT (100nM, 2h)	anti-PIAS3+PIAS1+PIAS2	2478	1686	-19.05	
LNCAP	TNF-alpha (1000 U/ml, 2h)	anti-PIAS3+PIAS1+PIAS2	97	69	-0.89	
LNCAP	TNF-alpha (1000 U/ml, 2h)	anti-PIAS3+PIAS1+PIAS2	86	66	-0.5	
LNCAP	TNF-alpha (1000 U/ml, 2h)	anti-PIAS3+PIAS1+PIAS2	880	460	-21.4	
LNCAP	TNF-alpha (1000 U/ml, 2h)	anti-PIAS3+PIAS1+PIAS2	810	485	-12.41	
LNCAP	TNF-alpha (1000 U/ml, 2h)	anti-p65	21	6	-1.93	
LNCAP	TNF-alpha (1000 U/ml, 2h)	anti-p65	21	7	-1.66	
LNCAP	TNF-alpha (1000 U/ml, 2h)	anti-p65	180	80	-7.14	
LNCAP	TNF-alpha (1000 U/ml, 2h)	anti-p65	168	76	-6.47	
LNCAP	DHT (100nM, 2h) + TNF-alpha (1000U/ml, 2h)	anti-p65	2075	1004	-61.01	
LNCAP	DHT (100nM, 2h) + TNF-alpha (1000U/ml, 2h)	anti-p65	2015	961	-61.49	
LNCAP	DHT (100nM, 2h) + TNF-alpha (1000U/ml, 2h)	anti-p65	2127	1041	-60.68	

LNCAP	DHT (100nM, 2h) + TNF-alpha (1000U/ml, 2h)	anti-p65	2008	1011	-53.12	
HUVEC	TNF-alpha (10 ng/ml, 30min)	anti-Pol3	867	50	-155.12	GSE34500
HUVEC	TNF-alpha (10 ng/ml, 30min)	anti-p65	15779	1040	-300	
IMR90	DMSO	H3K4me3 ChIP	15429	4242	-300	
IMR90	Nutlin-3a	H3K4me3 ChIP	14800	3896	-300	
IMR90	DMSO	H3K4me1 ChIP	13573	2528	-300	
IMR90	Nutlin-3a	H3K4me1 ChIP	1967	286	-300	
IMR90	DMSO	H3K27ac ChIP	15455	3236	-300	
IMR90	Nutlin-3a	H3K27ac ChIP	13167	2666	-300	
IMR90	DMSO	H4K16ac ChIP	3098	550	-300	
IMR90	Nutlin-3a	H4K16ac ChIP	1303	211	-192.97	
IMR90	DMSO	RNAPII ChIP	13161	2757	-300	
IMR90	Nutlin-3a	RNAPII ChIP	9070	1713	-300	
IMR90	DMSO	p53 ChIP	97	65	-2.62	
IMR90	Nutlin-3a	p53 ChIP	1637	734	-93.36	
IMR90	DMSO	H3K4me2 ChIP	27136	7113	-300	
IMR90	Nutlin-3a	H3K4me2 ChIP	25274	6516	-300	
MCF7	E2 for 45m	ERa	20417	8637	-300	[7]
MCF7	E2 for 45m	ERa	4268	1069	-300	
MCF7	IL1b for 45m	ERa	2813	911	-232.08	
MCF7	IL1b for 45m	ERa	62	7	-10.75	
MCF7	TNFa for 45m	ERa	5196	1538	-300	
MCF7	TNFa for 45m	ERa	45	15	-4.19	
MCF7	IKK7	ERa	1280	240	-166.56	
MCF7	IL1b+IKK7	ERa	19	6	-2.06	
MCF7	IKK7	ERa	57	42	-1.07	
MCF7	IL1b+IKK7	ERa	24	46	-1.78	
MCF7	E2+ICI	ERa	3739	540	-300	
MCF7	IL1b+ICI	ERa	1564	435	-151.48	
MCF7	E2+ICI	ERa	4	2	-0.36	
MCF7	IL1b+ICI	ERa	3328	1129	-259.85	
MCF7	E2+ICI	ERa	587	114	-75.34	
MCF7	IL1b+ICI	ERa	4520	819	-300	
MCF7	IL1b+ICI	ERa	1203	228	-155.61	
MCF7	E2 for 45m	p65	190	46	-21.49	
MCF7	E2 for 45m	p65	2	0	-0.53	
MCF7	IL1b for 45m	p65	244	50	-30.78	
MCF7	IL1b for 45m	p65	1560	322	-190.96	
MCF7	TNFa for 45m	p65	1534	437	-145.27	

MCF7	TNFa for 45m	p65	3175	1029	-261.56	
MCF7	Dexamethasone	GR E-20X sc-1003 Santa Cruz	8474	4131	-300	[8]
MCF7	Dexamethasone	GR E-20X sc-1003 Santa Cruz	6377	4410	-100.34	
MCF7	17ÃŸ-estradiol	ER cocktail: Ab-10 Thermo Scientific Lab Vision, HC-20 sc-543 Santa Cruz	4375	861	-300	
MCF7	17ÃŸ-estradiol	ER cocktail: Ab-10 Thermo Scientific Lab Vision, HC-20 sc-543 Santa Cruz	11153	4080	-300	
MCF7	Dexamethasone	FoxA1	6315	4018	-136.68	
MCF7	Dexamethasone	FoxA1	238	97	-15.29	
MCF7	17ÃŸ-estradiol	FoxA1	9178	7561	-53.4	
MCF7	17ÃŸ-estradiol	FoxA1	845	215	-89.05	
T47D	Dexamethasone	GR E-20X sc-1003 Santa Cruz	570	91	-74.81	
T47D	Dexamethasone	GR E-20X sc-1003 Santa Cruz	451	85	-54.06	
T47D	17ÃŸ-estradiol	ER cocktail: Ab-10 Thermo Scientific Lab Vision, HC-20 sc-543 Santa Cruz	2854	654	-293.27	
T47D	17ÃŸ-estradiol	ER cocktail: Ab-10 Thermo Scientific Lab Vision, HC-20 sc-543 Santa Cruz	3052	741	-299	
T47D	Dexamethasone	FoxA1	244	46	-29.61	
T47D	Dexamethasone	FoxA1	156	34	-17.44	
T47D	17ÃŸ-estradiol	FoxA1	303	42	-42.94	
T47D	17ÃŸ-estradiol	FoxA1	3266	903	-283.95	
T47D	Dexamethasone and 17ÃŸ-estradiol	FoxA1	12949	2332	-300	
K562	IFNa30	pol2	739	73	-117.62	ENCODE
K562	IFNa6h	pol2	838	86	-131.65	
K562	IFNg30	pol2	1342	152	-203.26	
K562	IFNg6h	pol2	1113	116	-173.65	
K562	IFNa30	cjun	2788	409	-300	
K562	IFNa6h	cjun	922	112	-136.38	
K562	IFNg30	cjun	2518	331	-300	
K562	IFNg6h	cjun	1583	232	-215.33	
K562	IFNa30	cmyc	3188	287	-300	
K562	IFNa6h	cmyc	5150	489	-300	
K562	IFNg30	cmyc	21370	2329	-300	

K562	IFNg6h	cmyc	11871	1181	-300	
GM12878	TNF	NFKB	4952	610	-300	

Supplementary Table 6. Binding site induction and compartmentalization in two cell lines under the same treatment, for a particular TF.

	AA	AB	BA	BB	total	A/B Enrichment	R	p-value
MCF7 - T47D; Treatment: Estradiol Antibody: ER [8]								
Replicate 1								
Cell1_only_BSs	2354	522	230	534	3640	2.33	1.99	7.06E-23
Cell2_only_BSs	1177	149	233	295	1854	1.63		
Common BSs	1344	158	103	144	1749			
Replicate 2								
Cell1_only_BSs	7302	1834	1229	2751	13116	1.56	1.5	6.41E-13
Cell2_only_BSs	854	108	177	180	1319	1.63		
Common BSs	1794	248	227	317	2586			
Two rep combined								
Cell1_only_BSs	9656	2356	1459	3285	16756	1.61	1.61	3.29E-29
Cell2_only_BSs	2031	257	410	475	3173	1.6		
Common BSs	3138	406	330	461	4335			
LNCAP - MCF7; Treatment: TNFa; Antibody: p65 [6]								
Cell1_only_BSs	74	28	16	43	161	1.7	1.59	0.0014
Cell2_only_BSs	1194	166	262	271	1893	1.56		
Common BSs	67	11	12	12	102			
HUVEC - MCF7; Treatment: TNFa; Antibody: p65. Genome-wide maps of RNA Polymerase II and p65 localization in HUVECs stimulated with TNF alpha (GSE34500)								
Cell1_only_BSs	12443	2568	321	842	16174	8	6.47	4.70E-99
Cell2_only_BSs	671	100	154	227	1152	1.44		
Common BSs	690	83	34	54	861			
LNCAP – HUVEC; Treatment: TNFa; Antibody: p65 [6]								
Cell1_only_BSs	75	39	28	39	181	1.47	8.73	1.62E-37
Cell2_only_BSs	12237	374	3470	866	16947	10		
Common BSs	60	7	12	4	83			

Supplementary Table 7. Preference of induced genes to the A compartment

Cell line	treatment	induced in A	induced in B	Log p-value	A/B enrichment	source
GM12878	TNF-a	3866	267	-101.57	3.76	ENCODE
IMR90	TNF-a (10ng/mL) 1hr	439	103	-6.43	1.74	[5]
IMR90	TNF-a (10ng/mL) 1hr	105	23	-2.12	1.82	
IMR90	cycloheximide (5Âµg/mL) pretreat 30min	254	46	-6.61	2.23	
IMR90	TNF-a (10ng/mL) 1hr; cycloheximide (5Âµg/mL) pretreat 30min	389	77	-8.39	2.06	
IMR90	TNF-a (10ng/mL) 1hr	80	27	-0.37	1.19	
HUVEC	IFN-G (50ng/mL) 2hr	124	10	-3.65	3.02	
MCF7	Estradiol (100nM) 160min	121	13	-3.73	2.75	
IMR90	Nutlin-3a	1771	558	-161.62	1.27	
MCF7	E2 for 3h	131	16	-3.49	2.45	[7]
MCF7	E2 for 3h	129	12	-4.51	3.16	
MCF7	IL1b for 3h	166	20	-4.4	2.51	
MCF7	IL1b for 3h	172	27	-3.07	1.95	
MCF7	IL1b+ICI for 3h	204	31	-3.79	2.02	
MCF7	IL1b+ICI for 3h	182	32	-2.56	1.75	
MCF7	TNFa for 3h	338	62	-3.99	1.7	
MCF7	TNFa for 3h	348	78	-2.12	1.4	
MCF7	TNFa+ICI for 3h	895	235	-1.82	1.2	
MCF7	TNFa+ICI for 3h	1045	382	-1.76	0.86	
MCF7	E2	252	31	-6.31	2.5	
MCF7	E2	421	35	-15.06	3.7	
MCF7	E2+TOT	511	62	-12.42	2.57	
MCF7	E2+TOT	62	2	-3.67	6.64	
MCF7	E2+TOT+IL1b	469	62	-10.19	2.36	
MCF7	E2+TOT+IL1b	495	57	-12.87	2.7	
MCF7	E2+TOT+TNFa	471	50	-13.45	2.92	
MCF7	E2+TOT+TNFa	404	56	-8.26	2.25	
LNCAP	TNF-alpha (1000 U/ml, 2h)	148	47	-0.26	1.1	
LNCAP	TNF-alpha (1000 U/ml, 2h)	158	47	-0.49	1.18	
LNCAP	DHT (100nM, 2h) + TNF-alpha (1000U/ml, 2h)	161	49	-0.42	1.15	
LNCAP	DHT (100nM, 2h) +	175	59	-0.11	1.04	

	TNF-alpha (1000U/ml, 2h)					
LNCAP	DHT (100nM, 2h)	64	8	-2.22	2.57	
LNCAP	DHT (100nM, 2h)	65	14	-0.94	1.57	

Supplementary Table 8. Promoters of induced genes are involved, in basal condition, in higher numbers of chromatin interactions.

Cell line	Treatment	Data type	Mean number of promoter interactions in the positive set	Mean number of promoter interactions in random sets	p-val
HUVEC	IFN	Hi-C	1.46	0.92	<10E-04
HUVEC	TNFa	Hi-C	1.57	0.95	<10E-04
K562	SAHA	ChIA-PET	5.44	3.34	<10E-04
K562	SAHA	Hi-C	1.12	0.91	<10E-04
K562	NaBut	ChIA-PET	5.27	3.37	<10E-04
K562	NaBut	Hi-C	1.03	0.92	0.0047
HMEC	TNFa	Hi-C	1.4	0.86	<10E-04
MCF7	IL1B	ChIA-PET	7.91	4.52	<10E-04
MCF7	E2 + ICI	ChIA-PET	4.75	4.53	0.41
MCF7	E2+TNFa	ChIA-PET	7.16	4.53	<10E-04
MCF7	E2	ChIA-PET	4.94	4.53	0.04
MCF7	E2+IL1b	ChIA-PET	7.51	4.52	<10E-04
MCF7	E2	ChIA-PET	8.16	4.53	<10E-04
MCF7	IL1b+ICI	ChIA-PET	7.67	4.52	<10E-04
MCF7	TNFa	ChIA-PET	7.27	4.52	<10E-04
MCF7	E2	ChIA-PET	10.63	4.53	<10E-04
MCF7	TNFa+ICI	ChIA-PET	6.89	4.53	<10E-04

IMR90	Nutlin-3a	Hi-C	1.21	0.86	<10E-04
IMR90	TNFa	Hi-C	1.25	0.86	<10E-04
IMR90	TNFa+cycloheximide	Hi-C	1.24	0.86	<10E-04
GM12878	TNFa	ChIA-PET	3.91	1.81	<10E-04
GM12878	TNFa	Hi-C	1.77	1.27	<10E-04

Supplementary Table 9. Preference of cell-type specific induced genes to cell-type specific A compartment

HMEC - MCF7									
	AA	AB	BA	BB	total	R	Enrichment		p-value
only induced in cell line 1	29	20	6	9	64	3.44	2.0		0.000952
only induced in cell line 2	267	22	36	33	358	1.67			
induced in both	34	4	1	4	43				
IMR90 - MCF7									
	AA	AB	BA	BB	total	R	Enrichment		p-value
only induced in cell line 1	312	58	65	26	461	0.93	1.52		0.000115
only induced in cell line 2	193	19	70	30	312	3.67			
induced in both	62	7	13	7	89				
GM12878 - IMR90									
	AA	AB	BA	BB	total	R	Enrichment		
only induced in cell line 1	3160	555	130	298	4143	4.33	3.21		
only induced in cell line 2	280	55	38	19	392	0.71			1.49E-06
induced in both	121	30	0	7	158				
GM12878 - MCF7									
	AA	AB	BA	BB	total	R	Enrichment		p-value
only induced in cell line 1	3315	443	243	187	4188	1.83	1.78		0.003586
only induced in cell line 2	213	22	28	25	288	1.25			
induced in both	92	16	5	0	113				

HUVEC - MCF7									
	AA	AB	BA	BB	total	R	Enrichment		p-value
only induced in cell line 1	28	20	2	2	52	9.5	2.0		7.34E-05
only induced in cell line 2	273	26	36	31	366	1.43			
induced in both	27	3	2	3	35				
HMEC - GM12878									
	AA	AB	BA	BB	total	R	Enrichment		p-value
only induced in cell line 1	35	17	7	6	65	2.36	3.4		7.44E-08
only induced in cell line 2	3437	112	388	322	4259	3			
induced in both	35	0	6	1	42				
HUVEC - GM12878									
	AA	AB	BA	BB	total	R	Enrichment		p-value
only induced in cell line 1	33	16	4	1	54	4.29	1.64		0.000288
only induced in cell line 2	3621	136	213	298	4268	1.67			
induced in both	29	0	3	1	33				
HMEC - IMR90									
	AA	AB	BA	BB	total	R	Enrichment		p-value
only induced in cell line 1	24	9	3	7	43	3	0.67		0.471484
only induced in cell line 2	354	60	33	39	486	0.58			
induced in both	46	8	6	4	64				

HUVEC - IMR90									
	AA	AB	BA	BB	total	R	Enrichment		p-value
only induced in cell line 1	31	12	1	3	47	13	0.47		0.019836
only induced in cell line 2	385	69	21	35	510	0.29			
induced in both	32	3	1	4	40				
HUVEC - HMEC									
	AA	AB	BA	BB	total	R	Enrichment		p-value
only induced in cell line 1	38	11	2	2	53	5.25	1.67		0.236958
only induced in cell line 2	59	7	4	3	73	0.5			
induced in both	24	5	0	5	34				

References

1. Barutcu AR, Lajoie BR, McCord RP, Tye CE, Hong D, Messier TL, Browne G, van Wijnen AJ, Lian JB, Stein JL, et al: **Chromatin interaction analysis reveals changes in small chromosome and telomere clustering between epithelial and breast cancer cells.** *Genome Biol* 2015, **16:**214.
2. Taberlay PC, Achinger-Kawecka J, Lun AT, Buske FA, Sabir K, Gould CM, Zotenko E, Bert SA, Giles KA, Bauer DC, et al: **Three-dimensional disorganization of the cancer genome occurs coincident with long-range genetic and epigenetic alterations.** *Genome Res* 2016, **26:**719-731.
3. Rao SS, Huntley MH, Durand NC, Stamenova EK, Bochkov ID, Robinson JT, Sanborn AL, Machol I, Omer AD, Lander ES, Aiden EL: **A 3D map of the human genome at kilobase resolution reveals principles of chromatin looping.** *Cell* 2014, **159:**1665-1680.
4. Le Dily F, Bau D, Pohl A, Vicent GP, Serra F, Soronellas D, Castellano G, Wright RH, Ballare C, Filion G, et al: **Distinct structural transitions of chromatin topological domains correlate with coordinated hormone-induced gene regulation.** *Genes Dev* 2014, **28:**2151-2162.
5. Jin F, Li Y, Dixon JR, Selvaraj S, Ye Z, Lee AY, Yen CA, Schmitt AD, Espinoza CA, Ren B: **A high-resolution map of the three-dimensional chromatin interactome in human cells.** *Nature* 2013, **503:**290-294.
6. Malinen M, Niskanen EA, Kaikkonen MU, Palvimo JJ: **Crosstalk between androgen and pro-inflammatory signaling remodels androgen receptor and NF-kappaB cistrome to reprogram the prostate cancer cell transcriptome.** *Nucleic Acids Res* 2017, **45:**619-630.
7. Stender JD, Nwachukwu JC, Kastrati I, Kim Y, Strid T, Yakir M, Srinivasan S, Nowak J, Izard T, Rangarajan ES, et al: **Structural and Molecular Mechanisms of Cytokine-Mediated Endocrine Resistance in Human Breast Cancer Cells.** *Mol Cell* 2017, **65:**1122-1135 e1125.
8. Swinstead EE, Miranda TB, Paakinaho V, Baek S, Goldstein I, Hawkins M, Karpova TS, Ball D, Mazza D, Lavis LD, et al: **Steroid Receptors Reprogram FoxA1 Occupancy through Dynamic Chromatin Transitions.** *Cell* 2016, **165:**593-605.